Delivery of aged terrestrial organic matter to the Laptev Sea during the last deglaciation

Arnaud Nicolas[1,2], Jens Hefter[1], Hendrik Grotheer[1], Tommaso Tesi[3], Ruediger Stein[1,2,4,5], Alessio Nogarotto[3],

Eduardo Queiroz Alves[1], Gesine Mollenhauer[1,2,4]

[1]Alfred Wegener Institute, Helmholtz Centre for Polar and Marine Research, Bremerhaven, Germany

[2]Department of Geosciences, University of Bremen, Bremen, Germany

[3]Institute of Polar Sciences, National Research Council, Bologna, Italy

[4]MARUM - Center for Marine Environmental Sciences, University of Bremen, Bremen, Germany

[5]Key Laboratory of Marine Chemistry Theory and Technology, Ocean University of China, Qingdao, China

Correspondence: Arnaud Nicolas (arnaud.nicolas@awi.de) and Gesine Mollenhauer
(gesine.mollenhauer@awi.de)

Abstract

Arctic warming is causing rapid thawing of permafrost, which holds about 1.25 times as much carbon as currently is present in the atmosphere. The ongoing Arctic warming and projected sea level rise are expected to accelerate permafrost thaw, leading to the reintroduction of ancient, previously frozen organic carbon into the contemporary carbon cycle. The degradation of permafrost and the consequent release of greenhouse gases into the atmosphere are considered one of the most significant positive climate feedback mechanisms that could potentially intensify global warming trends. Studying carbon release from permafrost thawing during the last deglaciation provides a perspective that can help refine the anticipated climate-permafrost feedback. However, the regional variations, timing and rate of carbon release from thawing permafrost remain elusive, primarily because of the limited number of deglacial records that document carbon mobilization occurrences. In the present study we analyzed a high-resolution marine sediment record from off the Lena River outflow located on the Laptev Sea continental slope, close to the paleo-shoreline during the Last Glacial Maximum, and we provided a continuous record of the last 16 kyr. Biomarkers and radiocarbon dating of terrestrial materials have been used to reconstruct deglacial permafrost thaw events. We integrated mass accumulation rate data from the core site with the depositional ages of terrigenous biomarkers to identify the occurrence of past massive permafrost degradation and mobilization. We found that the highest accumulation of strongly pre-aged terrigenous biomarkers coincided with peaks in rapid sea-level rise, suggesting that permafrost carbon delivered to the core site was mobilized mainly by coastal erosion. Superimposed on the coastal signal, a significant freshwater discharge event was documented at about 13 kyr BP, characterized by low mass accumulation rates of terrigenous biomarkers and relatively young pre-depositional ages compatible with surface runoff-derived terrigenous material. This study further adds to the limited datasets on the age of deglacial permafrost-derived carbon accumulating on the Arctic shelves and offers valuable insights into the future behavior of permafrost carbon soils in the context of a warming climate.

1 Introduction

Permafrost soils (0–3 m depth) in the Arctic region represent an important reservoir of carbon (C) stored as organic matter (OM) (~ 1000 Pg organic carbon (OC)) and are equivalent in size to about 1.25 times the level of C in the atmosphere today (Hugelius et al., 2014; Strauss et al., 2017). The Arctic has been warming nearly four times more rapidly than the global average temperatures (Rantanen et al., 2022). Future warming and sea level rise in the Arctic will exacerbate the permafrost thaw, thereby allowing the previously frozen ancient OM to be remobilized and in part degraded (Strauss et al., 2017). The subsequent release of greenhouse gases (carbon dioxide (CO_2) and methane (CH_4)) from degrading permafrost to the atmosphere is one of the most likely positive climate feedbacks that might amplify global warming (Schuur et al., 2008, 2009, 2015, 2022). Understanding the potential impact of permafrost thaw on climate is critical, yet the rates and mechanisms of carbon release from thawing require further characterization and quantification. Examining carbon release during past warming events can enhance our comprehension of permafrost feedback in relation to the warming expected during this century.

During the last deglaciation (~21 - 11 thousand years before the present [kyr BP]), the mobilization of ancient OM and subsequent release of C from permafrost is considered a significant contributing factor to the rapid increase in atmospheric greenhouse gas concentrations (Ciais et al., 2012; Köhler et al., 2014; Sabino et al., 2024; Simmons et al., 2016; Zimov et al., 2009). Yet, the regional occurrence, timing, and rate of carbon release from degrading permafrost during the last deglaciation are still poorly constrained because of the paucity of continuous climate reconstructions on carbon mobilization during the last deglaciation that are currently available from the Arctic (Keskitalo et al., 2017; Martens et al., 2019, 2020; Nogarotto et al., 2023; Tesi et al., 2016; Wu et al., 2022), sub-Arctic (Meyer et al., 2019; Winterfeld et al., 2018) and northern Europe (Alves et al., 2024). Moreover, the degree to which mobilized permafrost OM is remineralized is not well constrained either, and the available estimates differ widely (Bröder et al., 2018; Ruben et al., 2024; Tanski et al., 2019; Vonk et al., 2012).

The last deglaciation marked the transition from the Last Glacial Maximum (LGM) to the current Holocene era (<9.5 kyr BP). This transition period is characterized by abrupt changes in global climate, with an increase in atmospheric CO_2 concentrations of ~80 ppm (Marcott et al., 2014), a rapid rise in temperature of ~3.5 °C in the Northern Hemisphere amplified in the Arctic region (Shakun et al., 2012), and a global sea-level rise of 134 m from the melting and disappearance of the Arctic ice sheets (Lambeck et al., 2014). The Heinrich Stadial 1 (HS1) was a climatic event that happened during the last deglaciation, about 18.0 to 14.6 kyr BP, and was likely the result of iceberg discharges from the Laurentide ice sheet into the North Atlantic Ocean. The Bølling-Allerød (B/A; ca. 14.7 - 12.9 kyr BP) and the Pre-Boreal (PB; 11.5 – 9.5 kyr BP) were periods characterized by abrupt temperature increases in the Northern Hemisphere and their onsets coincide with periods of increased sea-level rise referred to as Meltwater Pulse 1A (mwp-1A) and Meltwater Pulse 1B (mwp-1B) respectively. The Younger Dryas (YD; 12.9 – 11.5 kyr BP) was a climate cooling phase that caused near-glacial conditions following the B/A warm period. The YD cold spell is believed to be driven by the catastrophic drainage of meltwater from Lake Agassiz, causing a significant reduction in the Atlantic Meridional Overturning Circulation (AMOC) and rapid sea-ice expansion (Broecker et al., 1985; Renssen et al., 2015).

The degradation of permafrost involves complex processes such as thawing and deepening of the active layer,
80   expansion of wetlands, and formation of thermokarst leading to subsidence, lake development, catastrophic
meltwater drainage, and coastal erosion (Mann et al., 2022; Vonk and Gustafsson, 2013). These processes liberate
82   previously freeze-locked, immobilized OM and sediments, rendering them susceptible to fluvial transport. With
warming temperatures, more precipitation and accelerated snowmelt occur, which enhance the erosive power of
84   waterways and their capacity to carry sediment loads (Hiyama et al., 2023). Moreover, rapid permafrost thaw can
generate catastrophic meltwater surges or thermokarst lake drainage events, causing sudden and significant
86   sediment mobilization and altering the Arctic landscape (Jorgenson and Grosse, 2016; Vonk and Gustafsson,
2013). Along Arctic coastlines, permafrost erosion is further intensified by the diminishing sea ice cover, which
88   exposes shorelines to wave action and storm surges. The interplay between thermal and mechanical erosion along
coastlines leads to accelerated shoreline retreat, introducing significant quantities of permafrost OM directly into
90   coastal waters (Vonk et al., 2012; Vonk and Gustafsson, 2013).

92   Terrigenous OM found in marine sediments often has an age that predates its deposition due to intermediate
storage in terrestrial reservoirs, such as permafrost soils, and the time taken for transport to the marine environment
94   (Bröder et al., 2018). This age difference, referred to as the pre-depositional age, provides insights into the time
scales associated with these terrestrial processes (Winterfeld et al., 2018). The OM derived from permafrost is
96   characterized by distinctly high pre-depositional ages due to its long-term preservation in frozen soils, allowing it
to be distinguished from other terrestrial inputs in marine sediments (Alves et al., 2024; Meyer et al., 2019;
98   Nogarotto et al., 2023; Winterfeld et al., 2018).

100   During the LGM, the Siberian Arctic region, including the modern Laptev Sea, was covered with continuous
permafrost (Lindgren et al., 2016; Vandenberghe et al., 2014). A reorganization of permafrost OC occurred after
102   the LGM, with a permafrost OC storage shift from loess and mineral soils to mostly peatlands in modern times
(Lindgren et al., 2018). As sea level dropped during the Pleistocene, the Ice Complex Deposits (ICD; also called
104   Yedoma deposits) (40 - 60 m thick) developed on the Laptev Sea, East Siberian Sea, and Chukchi Sea continental
shelves (Lindgren et al., 2018; Romanovskii et al., 2000). When sea-level rose again during deglaciation, the
106   inland and coastal permafrost were thawed, and the Yedoma deposits that were present on the continental shelves
were flooded and at least partially eroded. Different studies from the Arctic and sub-Arctic regions have suggested
108   that the biodegradation and oxidation of the thawed OC from Yedoma deposits have led to an increase in
atmospheric CO_2 concentrations (Martens et al., 2020; Meyer et al., 2019; Nogarotto et al., 2023; Tesi et al., 2016;
110   Winterfeld et al., 2018).

112   In this study, we present a high-resolution and well-dated continuous deglacial sedimentary record from core
PS2458-4 from the continental slope of the Laptev Sea. Previously, several studies have been carried out on the
114   OC component of core PS2458-4 to characterize various OC sources (marine versus terrigenous) and to interpret
the data sets in the context of paleoenvironmental changes (Boucsein et al., 2000, 2002; Fahl and Stein, 1999,
116   2012; Hörner et al., 2016; Stein et al., 2001, 2012; Stein and Fahl, 2004). Here, we analyzed terrigenous
biomarkers [lignin phenols; high-molecular-weight (HMW) *n*-alkanoic acids and branched glycerol dialkyl
118   glycerol tetraethers (brGDGTs)] and performed compound-specific radiocarbon analyses (CSRAs) on high-

molecular weight (HMW) *n*-alkanoic fatty acid methyl esters (FAMEs). Our results provide additional insights
120   into ancient carbon release from deglacial degradation of permafrost and contribute towards a better understanding
of permafrost thaw dynamics and aged carbon release for the projected warming climate and sea level rise.

122

2 Study area

124   The Laptev Sea is an open marginal sea of the Siberian Arctic Ocean sector, situated between the Kara and the
East Siberian Seas. It is bounded by the Taymyr Peninsula and the Severnaya Zemlya archipelago in the west and
126   the new Siberian Islands in the east (Fig. 1). The Laptev Sea shelf is shallow, sloping northward down to water
depths of ~50 m. The shelf is marked by the steep continental slope that reaches down to ~1700 m to the floor of
128   the Amundsen and Nansen basins at a depth of > 3000 m. With a catchment area of about 2.43×10^6 km^2, the
Lena is the second-largest river in the Arctic (with a modern total discharge volume of 588 km^3 yr^{-1}) and drains
130   extensive permafrost areas (consisting of 90 % of both continuous and discontinuous permafrost) into the Laptev
Sea (Holmes et al., 2012). Each year, the large rivers of the Laptev Sea, including the Lena, transport huge amounts
132   of OM onto the shelf (Fahl et al., 1999; Stein and Fahl, 2000). There are submarine channels on the Laptev Sea
shelf that were probably created by the large rivers from the hinterland when the sea level was lower during the
134   Late Pleistocene period (Holmes & Creager, 1974; Kleiber & Niessen, 1999). The deglacial sea level rise (Bauch
et al., 2001; Klemann et al., 2015) has caused the Laptev Sea shelf to undergo rapid coastal erosion and led to
136   remobilization of ancient OC from the labile permafrost coastline (Martens et al., 2020; Stein and Fahl, 2000;
Tesi et al., 2016). The Holocene shelf sediments in the Laptev Sea contain a mixture of both marine and terrestrial
138   OC, following the transformation of the shelf from a terrestrial to a marine environment after the last transgression
(Bauch et al., 1999; Fahl and Stein, 1999, 2012; Martens et al., 2020; Stein et al., 2001; Taldenkova et al., 2005;
140   Tesi et al., 2016). An event of significant surface water freshening occurred in the Laptev Sea at approximately
13 kyr BP, coinciding with the beginning of the YD period. This event was hypothesized to have resulted from
142   the drainage of ice-dammed lakes in the ancient Lena River system, as described in Spielhagen et al. (2005).
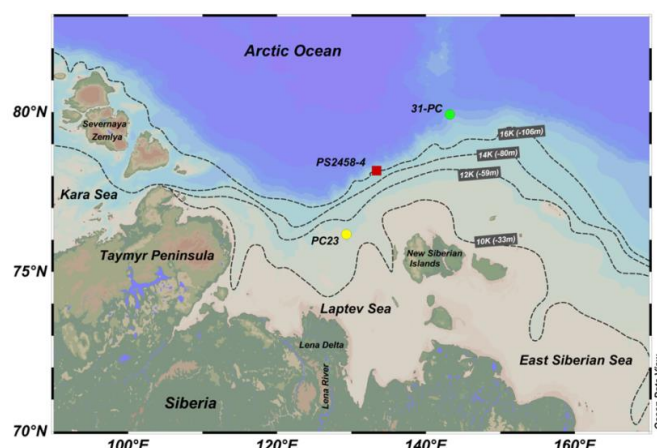

Figure 1. Map of the Laptev Sea shelf showing the location of core PS2458-4 (red square), PC23 (yellow circle) (Tesi et al., 2016), **and 31-PC (green circle)** (Martens et al., 2020)**. The dashed lines represent the reconstructed coastline extent at 4 different time periods (where 10K=10 kyr BP) with corresponding water depth values in meters shown in brackets** (Klemann et al., 2015)**. The map was created using Ocean Data View (Schlitzer, 2016).**

3 Materials and Methods

3.1 Core location and chronology

Kastenlot core PS2458-4 (78°10.0′N, 133°23.9′E) was recovered in 1993 during the ARK-IX/4 RV *Polarstern* Expedition from the eastern Laptev Sea continental margin at a water depth of 983 m, close to the Lena paleo-river submarine channel (Fütterer, 1993) (Fig. 1). The 8 m long core contains very dark olive-gray silty clay of dominantly terrigenous origin (Fütterer, 1993). The sediment core was stored frozen at -20 °C since recovery. We used archived sediment samples that were freeze-dried, homogenized and kept in amber glass jars for the biomarker and isotopic analyses. Sediment samples for compound-specific radiocarbon dating were sampled from the frozen core sections and were then freeze-dried and homogenized before extraction.

An updated chronology of core PS2458-4 was established by accelerator mass spectrometry (AMS) ^{14}C dating based on seven mixed benthic foraminifera dates from Spielhagen et al. (2005) and seven mixed foraminifera and bivalve samples (Nicolas et al., 2024) measured at the Mini Carbon Dating System (MICADAS) ^{14}C laboratory facility of the Alfred Wegener Institute (Mollenhauer et al., 2021). The radiocarbon and modelled ages, and species names of foraminifera and bivalve samples used are given in Nicolas et al. (2024). The age-depth model of core PS2458-4 was constructed using the OxCal 4.4 software (Ramsey, 2009). For this, the ^{14}C dates were calibrated with the Marine20 curve (Heaton et al., 2020), and a local marine reservoir correction (ΔR) value of 345 ± 60 ^{14}C years (Nicolas et al., 2024) based on a beryllium-based age model. The sediment interval between 121.5 and 667 cm represents the time between about 6.0 and 13.7 calendar kyr BP. The sediment layer at 0.5 cm represents a modern calendar age of 0, signifying the present-day reference point in the stratigraphic timeline. The base of the core at 800 cm has an extrapolated calendar age of about 15.6 calendar kyr BP.

3.2 Biomarker analyses

Total lipids were extracted from freeze-dried and homogenized sediment (1-3 g) using ultrasonic extraction with a mixture of dichloromethane:methanol (9:1, v/v). This procedure was performed three times and the combined resulting total lipid extracts (TLE) were saponified with 0.1 M potassium hydroxide in methanol:water (9:1) for 2 h at 80 °C. The extraction of neutral lipids was performed with *n*-hexane, and the pH of the remaining TLE solution was adjusted to 1 by adding HCl (37 %). The *n*-alkanoic acids were extracted with DCM and were then methylated using a mixture of HCl (37 %), and MeOH on a hot plate at 50 °C for 12 h, and *n*-hexane was used to extract the fatty acid methyl ester (FAME) fractions. The neutral lipids were extracted from the TLE with n-hexane. Column chromatography with silica gel was used to further separate the neutral lipids with n-hexane and DCM:MeOH (1:1, v/v), eluting the apolar and GDGT (polar) compounds, respectively. The FAMEs were analyzed using a 7890A gas chromatograph (GC) (Agilent Technologies) equipped with a flame ionization detector (FID) and DB-5MS fused silica capillary column (60 m, ID 250 μm, 0.25 μm film coupled to a 5 m, ID 530 μm deactivated fused silica pre-column).

GDGT fractions were filtered using a polytetrafluoroethylene syringe filter with a pore size of 0.45 μm. The analysis was undertaken using an Agilent 1200 series high-performance liquid chromatography system coupled via an atmospheric pressure chemical ionization interface to an Agilent 6120 mass spectrometer (HPLC-APCI-MS), with a method slightly modified from Hopmans et al. (2016).

184   Separation of GDGTs, including the 5 -/6-methyl isomers of brGDGTs, was achieved on two UPLC silica columns in series (Waters Acquity BEH HILIC, 2.1 × 150 mm, 1.7 µm), with a 2.1 × 5 mm pre-column of the same material

186   maintained at 30 °C. Mobile phases A and B consisted of n-hexane / chloroform (99:1, v/v) and n-hexane/2-propanol/chloroform (89:10:1, v/v/v), respectively. After sample injection (20 µL) and 25 min isocratic elution

188   with 18 % mobile phase B, the proportion of B was increased to 50 % within 25 min, and to 100 % within the next 30 min. After 5 min at 100 % B and before the analysis of the next sample, the column was re-equilibrated

190   with 18 % B for 15 min. The flow rate was 0.22 mL/min, resulting in a maximum back pressure of 220 bar. The total run time was 100 min.

192

    GDGTs were detected using positive ion APCI-MS and selective ion monitoring (SIM) of their $(M + H)^+$ ions

194   (Schouten et al., 2007). APCI spray-chamber conditions were as follows: nebulizer pressure 50 psi, vaporizer temperature 350 °C, N_2 drying gas flow 5 L / min and 350 °C, capillary voltage (ion transfer tube) -4 kV, and

196   corona current +5 µA. The MS-detector was set for SIM of the following $(M+H)^+$ ions: m/z 1302.3 (GDGT-0), 1300.3 (GDGT-1, OH-GDGT-0), 1298.3 (GDGT-2, OH-GDGT-1), 1296.3 (GDGT-3, OH-GDGT-2), 1292.3

198   (Crenarchaeol + regio-isomer), 1050 (brGDGT-IIIa/IIIa'), 1048 (brGDGT-IIIb/IIIb'), 1046 (brGDGT-IIIc/IIIc'), 1036 (brGDGT-IIa/IIa'), 1034 (brGDGT-IIb/IIb'), 1032 (brGDGT-IIc/IIc'), 1022 (brGDGT-Ia), 1020 (brGDGT-

200   Ib), 1018 (brGDGT-Ic) and 744 (C_{46} standard), with a dwell time of 57 ms per ion. Owing to the lack of appropriate standards, the individual response factors of the analyzed C_{86}-GDGTs relative to the C_{46}-GDGTs standard were

202   not evaluated, and the reported contents should be considered semi-quantitative.

204   The branched and isoprenoid tetraether (BIT) index was calculated as defined by Hopmans et al. (2004), but with the explicit inclusion of the 6-methyl brGDGTs (Sinninghe Damsté, 2016).

206

$$BIT = (Ia + IIa + IIa' + IIIa + IIIa') / (Ia + IIa + IIa' + IIIa + IIIa' + crenarchaeol)$$

208   Compounds Ia, IIa and IIIa are the basic and 5-methyl brGDGTs and IIa' and IIIa' are the 6-methyl brGDGTs, all together representing terrestrial inputs, and the isoprenoid GDGT crenarchaeol representing marine

210   Nitrososphaerota (formerly Crenarchaeota and Thaumarchaeota).

212   Long-chain n-alkanoic acids are derived from the leaf wax lipids of higher land plants (Eglinton & Hamilton, 1967). In higher plants, the predominant n-alkanoic acids are high-molecular-weight saturated fatty acids with

214   even-numbered carbon chains (Bianchi and Canuel, 2011). Branched GDGTs (brGDGTs) are derived from soil bacteria, and they serve as an indicator for the input of soil and riverine OM in marine sediments (Hopmans et al.,

216   2004; De Jonge et al., 2015). The BIT index (Hopmans et al., 2004) is used as a proxy to reconstruct terrigenous input to the ocean. It is based on the relative abundance of brGDGTs and the isoprenoid GDGT crenarchaeol,

218   where higher BIT values indicate more terrestrial OM input to the marine sediments (Weijers et al., 2006).

220

222

The ring index of hydroxylated tetraethers (RI-OH') and its derived sea surface temperature (SST) are calculated
224 based on the following equations (Lü et al., 2015):

226 $$RI - OH' = ([OH - GDGT - 1] + 2 \text{ x } [OH - GDGT - 2]) /$$
$$([OH - GDGT - 0] + [OH - GDGT - 1] + [OH - GDGT - 2]$$

228

$$RI - OH' = 0.0382 \text{ x } SST + 0.1 \ (R^2 \ 0.75, \ n=107; \ p<0.01)$$

230

Lignin is an organic polymer that is biosynthesized by vascular plants. The concentration of different phenolic
232 monomers from lignin varies between different plant types, and each type of phenol demonstrates unique
susceptibility to degradation (Cao et al., 2023; Feng et al., 2013; Hedges et al., 1988; Hedges and Mann, 1979;
234 Lobbes et al., 2000; Wild et al., 2022). The extraction of lignin phenols was carried out using alkaline CuO
oxidation following the method described in Goñi and Montgomery (2000). Sediment samples (200 mg) were
236 oxidized with an alkaline aqueous solution (2 M NaOH) under oxygen-free conditions in Teflon vessels using a
CEM Mars6 Microwave Digestion System (150 °C for 90 min). Following oxidation, the samples were placed
238 into Falcon tubes and, to estimate recovery rates, a known amount of internal standard (ethylvanillin) was added
to each sample. Samples were centrifuged, and the supernatant was acidified to pH 1 with HCl (37 %) and
240 extracted two times with ethyl acetate. The extracts were dried under a stream of N_2 and redissolved in pyridine.
The samples were then derivatized with N,O-Bis(trimethylsilyl) trifluoroacetamide (BSTFA) and 1 %
242 trimethylchlorosilane (TMCS) at 50 °C for 30 min. The analysis was carried out via gas chromatography-mass
spectrometry (GC-MS), using an Agilent 7820 A Gas Chromatograph coupled with a 5977B Mass Selective
244 Detector in single ion monitoring (SIM), fitted with a Trajan SGE 30 m x 320 μm (0.25 μm-thick film) PB-1
capillary column. The GC-MS column temperature ramp was set from 95 °C to 300 °C at a rate of 4 °C/min with
246 a hold time of 10 min. The measurement of lignin phenols was accomplished using external calibration curves,
which were developed using commercial standards obtained from Sigma-Aldrich.

248

In this study, we quantified eight lignin-derived phenols: vanillyl (V) (vanillin (Vl), acetovanillone (Vn), vanillic
250 acid (Vd)); syringyl (S) (syringaldehyde (Sl), acetosyringone (Sn), syringic acid (Sd)); and cinnamyl (C) phenols
(p-coumaric acid (p-Cd) and ferulic acid (Fd)). Ratios of different Cu-oxidation products can be used as proxies
252 for reconstructing vegetation types, inferring the contribution of different sources and their degradation (Hedges
et al., 1988; Hedges and Mann, 1979). Ratios of S/V and C/V are commonly used to infer the source of lignin
254 phenols and to differentiate between woody and non-woody tissues of angiosperms and gymnosperms (Hedges
and Mann, 1979). Ratios of Sd/Sl (represented as $(Ad/Al)_s$) and Vd/Vl (represented as $(Ad/Al)_v$) can be used to
256 investigate the decomposition state of lignin, where both ratios increase during aerobic decomposition through
oxidation (Ertel and Hedges, 1984; Hedges et al., 1988; Otto and Simpson, 2006).

258

3,5-dihydroxybenzoic acid (3,5Bd) is another oxidation product that is not necessarily derived from lignin but is
260 present in peat (Amon et al., 2012; Goñi et al., 2000). The 3,5Bd/V ratio reflects the degradation state of
terrigenous OM and can be used as a tracer for wetland extension. The C phenols p-Cd and Fd are both derived
262 from non-woody vascular plant tissues, such as grasses and many herbaceous tissues (Ertel and Hedges, 1984;

Hedges et al., 1988). The structural difference between *p*-Cd and Fd, namely the presence of a methoxyl group in

264 the latter, may explain the preferential degradation of Fd. Therefore, the *p*-Cd/Fd ratio has been employed as a

diagenetic indicator (Amon et al., 2012; Houel et al., 2006; Salvadó et al., 2016). A higher *p*-Cd/Fd ratio generally

266 indicates a more degraded state of lignin. In Arctic rivers, *p*-Cd/Fd is also used to differentiate surface soil organic

matter from deep root input (Feng et al., 2015).

268

Cutin, a biopolymer integral to the cuticles of vascular plants, is frequently utilized alongside lignin to assess

270 terrestrial contributions in sediment samples. When subjected to alkaline CuO oxidation, cutin produces eight

primary compounds: 16-hydroxyhexadecanoic acid (ω-C16), hexadecan-1,16-dioic acid (C16DA), 18-

272 hydroxyoctadec-9-enoic acid (ω-C18:1), 7- or 8-dihydroxy C16 α,ω-dioic acid (x-OH-C16DA), and 8-, 9-, or 10-

16-dihydroxy C16 acids (x,ω-OH-C16). The sum of these acids is indicative of the total cutin content within the

274 sample. The sources of cutin products are generally leaves, blades and needles of vascular plants (Goñi and

Hedges, 1990). The cutin/lignin ratio can be used to assess the degradation state of terrigenous OM. Since cutin

276 is usually more labile than lignin, the changes in the ratio can indicate preferential degradation. Furthermore, a

higher cutin to lignin ratio generally signifies a greater contribution from leaf and needle tissues compared to

278 woody tissue contribution.

280 **3.3 Bulk analyses**

The procedures employed for bulk analyses are described in Tesi et al. (2020). Total organic carbon (TOC), total

282 nitrogen (TN) content, and stable carbon isotope (δ^{13}C) composition were measured in 60 sediment samples.

About 20 mg of homogenized sediment was acidified with 1.5 N HCl in silver capsules to eliminate the inorganic

284 carbon. The analysis was performed with a Thermo Scientific FLASH 2000 CHNS/O analyzer coupled to a

DeltaO Thermo Fisher isotope ratio mass spectrometer (IRMS), located at the Stable Isotope Laboratory of ISP-

286 CNR. The δ^{13}C results are presented using the standard delta notation (‰). The isotopic data were calibrated using

the IAEA reference material IAEACH7 polyethylene (-32.15‰ vs. Vienna Pee Dee Belemnite (VPDB)). To

288 ensure measurement reproducibility, other standards were used with a sediment matrix throughout the analytical

runs. Based on replicate measurements of these sediment standards, the standard deviation for δ^{13}C measurements

290 was less than 0.1‰.

292 **3.4 Bulk organic carbon (OC) and compound-specific radiocarbon analyses (CSRA)**

The methods used for radiocarbon dating are described in Mollenhauer et al. (2021). Fifty-six sediment samples

294 were selected for bulk OC radiocarbon analysis (Supplementary Table S1). About 1 mg OC was weighed into

silver capsules, based on the TOC contents of sediment samples. The samples underwent three separate treatments

296 with 6 N hydrochloric acid (HCl) to completely eliminate the inorganic carbon fraction. The samples were dried

on a hot plate at 60 °C during acid addition and stored in an oven at 60 °C until analysis. The acidified and dried

298 sediment samples in the silver capsules were enclosed within tin capsules and then combusted using an Elementar

vario ISOTOPE Elemental Analyzer. The resulting oxidized carbon (CO_2) was directly graphitized using an

300 Ionplus AGE3 system (Automated Graphitization System) (Wacker et al., 2010a). Radiocarbon content analysis

was performed using an Ionplus MICADAS accelerator mass spectrometer (Synal et al., 2007; Wacker et al.,

302 2010b). Radiocarbon data were normalized against size-matched replicates of Oxalic Acid II (OxAII, NIST

304 SRM4990C) and blank corrected against ^{14}C-free phthalic anhydride (PhA, Sigma-Aldrich 320064, Lot# MLBZ4209V) processed alongside the samples using the BATS software (Wacker et al., 2010b).

306 Since the ^{14}C bulk dating values represent the ^{14}C content of a combination of compounds likely originating from both marine and terrestrial sources, compound-specific ^{14}C analyses of high-molecular-weight n-alkanoic acids

308 were further undertaken. These high-molecular-weight n-alkanoic acids ($C_{24:0}$, $C_{26:0}$, $C_{28:0}$, and $C_{30:0}$) are derived from vascular plants and their presence in marine sediments indicates pre-aged terrigenous OM export to the

310 oceans as reported in previous studies (Meyer et al., 2019; Nogarotto et al., 2023; Winterfeld et al., 2018; Wu et al., 2022).

312

For the compound-specific radiocarbon dating of the high-molecular-weight n-alkanoic acids, freeze-dried and

314 homogenized sediment samples (40 –100 g) from 18 selected depths (Supplementary Table S2) were extracted with dichloromethane:methanol (9:1, v/v) using a Soxhlet for over 48 hours. The total lipid extracts were

316 saponified with 0.1 M potassium hydroxide in MeOH:water 9:1 for 2 h at 80 °C. Following saponification, extraction of neutral lipids was done with n-hexane, and the n-alkanoic acids were extracted with DCM after the

318 pH was adjusted to 1 by adding HCl (37 %). The n-alkanoic acids were then methylated using a mixture of HCl (37 %) and MeOH with a known ^{14}C signature, under a nitrogen atmosphere at 50°C overnight.

320

The resulting fatty acid methyl esters (FAMEs) were extracted using n-hexane and separated from polar

322 compounds via silica gel chromatography. The n-$C_{26:0}$, n-$C_{28:0}$ and n-$C_{30:0}$ alkanoic acids underwent additional purification using preparative capillary gas chromatography (PC-GC) (Eglinton et al., 1996). This process utilized

324 an Agilent 6890N GC system equipped with a Gerstel Cooled Injection System and a preparative fraction collector (Kusch et al., 2010). The GC was fitted with a Restek Rxi-1ms fused silica capillary column (30m, 0.53mm ID,

326 1.5µm film). The purity and recovery of each FAME fraction was assessed on a small sub-sample using gas chromatography flame ionization detection (GC-FID).

328

Purified FAMEs were then transferred using dichloromethane to 25 µL tin capsules for analysis and thoroughly

330 dried. Samples were combusted in an Elementar Vario ISOTOPE Elemental Analyzer, and the resulting CO_2 was analyzed for ^{14}C / ^{12}C ratios using an AMS system equipped with a gas-ion source (MICADAS). The radiocarbon

332 data was normalized against OxAII standard gas (CO_2 produced from OxAII, NIST SRM4990C) and primary blank corrected against ^{14}C-free CO_2 reference gas using the BATS software (Wacker et al., 2010b).

334

All results are presented as fractions of modern carbon ($F^{14}C$). The approach described in Sun et al. (2020) was

336 used to undertake corrections for the procedural blank. To achieve this, in-house reference samples of ^{14}C-free Messel shale ($F^{14}C = 0$) and modern apple peel ($F_m = 1.029 \pm 0.001$) were subjected to the same pre-treatment as

338 our unknown age samples. To account for the methyl group added during sample derivatization, isotopic mass balance was employed for correction, and all uncertainties were fully propagated throughout the process

340 (Winterfeld et al., 2018).

342

3.5 Pre-depositional ages of terrigenous organic carbon

344   The pre-depositional age of terrigenous organic carbon was calculated based on the equations employed by Schefuß et al. (2016) and also given by Winterfeld et al. (2018), Wu et al. (2022), and Alves et al. (2024). The

346   initial radiocarbon content ($\Delta^{14}C_{inital}$), that is the radiocarbon content before the organic carbon was deposited in the sediment, is calculated as follows:

348

$$\Delta^{14}C_{inital} = (F^{14}C \ e^{\lambda t} - 1) \times 1000 ‰$$

350

where $F^{14}C$ is the measured fraction of modern carbon and the blank- and methanol-corrected F_m values are

352   employed for compound-specific samples; λ is a decay constant (1/8267 yr^{-1}), and t is the time of deposition derived from the sediment age model. The $\Delta^{14}C$ values of the atmosphere contemporaneous with the compounds

354   ($\Delta^{14}C_{atm}$) were obtained from comparison with the IntCal20 dataset (Reimer et al., 2020) using the age ranges given by the age model for the respective depths. The pre-depositional ^{14}C ages for the compound-specific samples

356   were calculated with the following equation:

358    $$\text{pre-depositional age} = -8033 \times \ln [(1 + \Delta^{14}C_{initial} / 1000) / (1 + \Delta^{14}C_{atm} / 1000)]$$

360

3.6 Mass accumulation rates

362   The mass accumulation rates (MARs) of the terrigenous biomarkers are calculated as follows:

$$MAR = SR \times DBD \times BM$$

364   where SR = sedimentation rate (cm kyr^{-1}); DBD = dry bulk density (g cm^{-3}); BM = biomarker content ($\mu g \ g^{-1}$ sed/ mg g^{-1} OC).

366

The SR data (Fig. S1a) are obtained after generating the age-depth model from OxCal4.4 software. The DBD data

368   used are from Spielhagen et al. (2005). The BMs are calculated for each biomarker as follows:

- n-alkanoic acids ($\mu g \ g^{-1}$ sed): sum of contents of n-$C_{26:0}$, n-$C_{28:0}$ and n-$C_{30:0}$,

370   - brGDGTs ($\mu g \ g^{-1}$ sed): sum of contents of brGDGT-Ia, brGDGT-IIa\IIa' and brGDGT-IIIa\IIIa',

- lignin and cutin (mg g^{-1} OC): sum of the content of the eight lignin phenols ($\sum 8_{lignin}$) and eight cutin-

372   derived acids ($\sum 8_{cutin}$) respectively.

374   **4 Results**

The updated age-depth model indicated distinct variations in sedimentation rates across different climatic periods.

376   Elevated sedimentation rates were observed during the warm B/A and PB intervals, with peak values reaching 0.16 cm yr^{-1} in both periods. These peaks in sedimentation coincided with periods of rapid sea-level rise and

378   occurred immediately following mwp-1A and mwp-1B (Fig. S1a, d). In contrast, the cold YD period showed markedly lower sedimentation rates, ranging from 0.05 to 0.07 cm yr^{-1}. Subsequently, the Holocene was

380   characterized by a progressive decline in sedimentation rates due to the increase in distance between the core location and the sediment source, ultimately stabilizing at considerably lower values of about 0.02 cm yr^{-1}. Our

382   data do not indicate the existence of a hiatus at 100 cm (~5 kyr BP) as speculated by Spielhagen et al. (2005). A

384   previous study has also supported the use of an age model for core PS2458-4 without a hiatus from the mid to the
       late Holocene period (Fahl and Stein, 2012).

386   We used the BIT index to reconstruct terrestrial OM input into the ocean sediments and higher values were
       observed during the HS1-B/A and part of the YD (~11.9 - 15.6 kyr BP) with a mean value of 0.70, indicating
388   more terrigenous input to the Laptev Sea sediments (Fig. 2a). Following a decline in the BIT index during the
       YD, values slightly increased during the PB period. Subsequently, the values decreased and remained low and
390   relatively constant (mean value = 0.18; n=31) throughout the Holocene, suggesting a more pronounced
       accumulation of marine-derived organic matter at the core site. The highest MARs of terrigenous biomarkers
392   (HMW n-alkanoic acids, brGDGTs, and lignin) (Figs. 2 b, c, d) were noted during the B/A and PB, decreasing
       during the YD cold spell and with low and rather constant values observed during the Holocene period. The
394   terrigenous biomarker maximum observed during the B/A was more pronounced than during the PB, with an
       additional less evident peak observed during the HS1. The MARs of lignin phenols and cutin-derived products
396   both indicate maxima in values during the B/A and the PB periods, with a decrease in values during the YD (Fig.
       2d). During the Holocene, the MARs of both biopolymers decreased and reached low and constant values. The
398   MAR values of lignin phenols exhibited higher values compared to the MAR values of the cutin-derived products.

400   The pre-depositional ages of the bulk OC record (Fig. 2e; Table S1) show the highest values during the HS1-B/A
       (~13.2 – 18.5 ^{14}C kyr), decrease into the YD and rise again during the PB with values in the range from ~12.7 –
402   15.4 ^{14}C kyr. The values then decline towards the Holocene, reaching relatively low and constant values varying
       from ~5.7 to 7.5 ^{14}C kyr during the most recent time (< 5 kyr BP). The compound-specific radiocarbon analyses
404   of the HMW n-alkanoic acids (C$_{26:0}$ and C$_{28:0}$) indicated that during the HS1- B/A, the terrigenous biomarkers
       were pre-aged by ~17.1 to 21.1 ^{14}C kyr at the time of deposition (Fig. 2f; Table S2). High pre-depositional ages
406   are also observed during the PB, with values ranging from 17.9 to 21.5 ^{14}C kyr. The youngest pre-depositional
       ages of ~8.8 to 10.5 ^{14}C kyr were recorded during the YD. The values became progressively younger during the
408   Holocene and were pre-aged by ~ 12.4 to 18.4 ^{14}C kyr. The oldest pre-depositional ages align with the maxima in
       terrigenous deposition that occurred during the B/A and the PB, which further coincide with periods of rapid sea
410   level rise (Fig 2l) (Lambeck et al., 2014). The bulk δ^{13}C record (Fig. 2g) indicates an average ratio of about -25.0
       ‰ during both the HS1-B/A and the PB, which typically represents more terrigenous OC input in marine sediment
412   during these warm periods. The bulk δ^{13}C average value was about -24.2 ‰ during the YD, and the values then
       become more positive towards the Holocene, implying a predominance of marine-derived OM.

414

       The concentrations of lignin phenols exhibited distinct temporal variations throughout the studied period (Fig.
416   3b). High concentrations were observed during the HS1-B/A interval, followed by a significant decrease during
       the mid-YD phase. A subsequent increase occurred during the YD-PB transition, culminating in a prominent
418   maximum. As the Holocene progressed, lignin phenol concentrations diminished, stabilizing at lower, relatively
       constant values. Cutin-derived products demonstrated a similar trend as lignin phenols, displaying a pronounced
420   maximum coinciding with the YD-PB period, although at lower overall concentrations (Fig. 3a).

422 The S/V ratio was relatively low during the HS1-B/A interval, followed by an increase during the YD (Fig. 3d, 4). After a decrease during the YD-PB transition, the S/V ratio increased during the Holocene. A similar trend

424 was observed for the C/V ratio, which also increased during the Holocene, although its peak during the YD period was less pronounced than that of the S/V ratio (Fig. 3c, d). The $(Ad/Al)_v$ and $(Ad/Al)_s$ followed similar trends

426 with the highest values occurring during the Holocene and less pronounced maxima occurring during the YD and the HS1-B/A period (Fig. 3f, g). The cutin/lignin ratio showed maximum values during the YD and relatively

428 lower values during the B/A and PB periods. A general decrease in p-Cd/Fd values was observed during the YD, with a maximum occurring during the Holocene and with less prominent peaks observed during the B/A and PB.

430 The 3,5Bd/V ratio exhibited the highest values during the YD, with less pronounced maxima during the Holocene (Fig. 3i).

432

The reconstructed RI–OH'–SSTs showed the highest values during the B/A and HS1 periods with an average of

434 ~ 0.7 °C (Fig. 2m). The values then decreased into the YD, when the lowest values were recorded. This trend towards colder SST values is also very well reflected in the HBI record determined in core PS2458-4, that is, the

436 diene/IP$_{25}$ ratio (Stein et al., 2012). The reconstructed SST values showed a small increase during the PB and then stayed low during the Holocene, averaging around -1.2 °C.
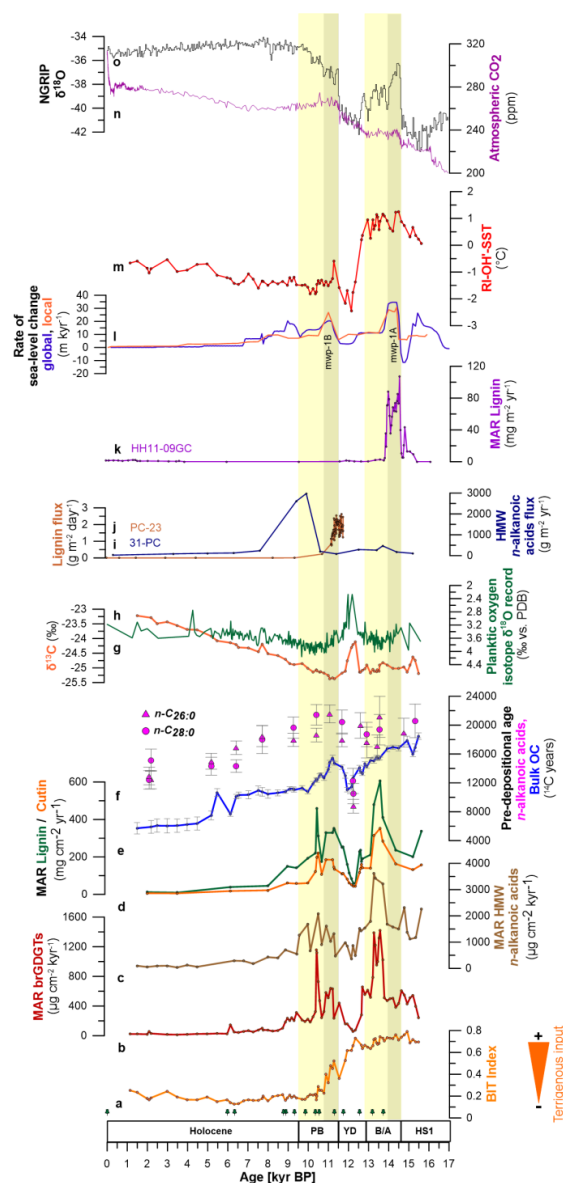
438

440

442

Figure 2. (a) BIT index record. (b) MAR brGDGTs. (c) MAR HMW *n*-alkanoic acids. (d) MAR Lignin (green) / Cutin (orange). (e) ¹⁴C bulk sediment OC. (f) Age at deposition of HMW *n*-alkanoic acids (C₂₆:₀ and C₂₈:₀). (g) δ¹³C values. (h) Planktic δ¹⁸O record plotted on new age-depth model with ΔR value of 345 ± 60 ¹⁴C years (Spielhagen et al., 2005). (i) HMW- n-alkanoic acids flux from core 31-PC (Martens et al., 2020). (j) Lignin flux from core PC23 (Tesi et al., 2016). (k) MAR Lignin from core HH11-09GC (Nogarotto et al., 2023). (l) Rate of sea-level change, global (Lambeck et al., 2014), local (Klemann et al., 2015). (m) Sea surface temperature proxy RI'-OH-SST. (n) NGRIP δ¹⁸O (Andersen et al., 2004). (o) Atmospheric CO₂ (Köhler et al., 2017). Yellow bands represent the warm phases Bølling-Allerød (B/A) and Pre-Boreal (PB). Gray bands indicate the timing of mwp-1A and mwp-1B (Lambeck et al., 2014). The pin marks at the bottom represent the age control points of core PS2458-4.
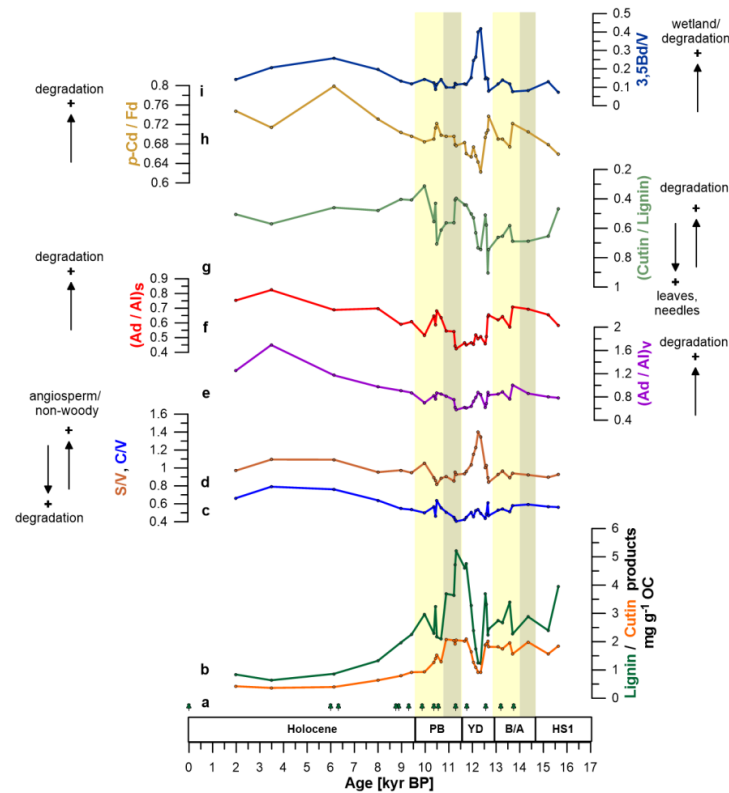
Figure 3. (a) Concentration of cutin products (orange.) (b) Concentration of lignin products (green). (c, d) S/V and C/V ratios reflect the degree of lignin degradation and/or vegetation change. (e, f) Ad/Al ratio represents the degradation of lignin phenols. (g) Cutin / Lignin. (h) *p*-Cd / Fd. (i) 3,5 Bd/V ratio reflects wetland expansion or degree of degradation. Yellow bands represent the warm phases Bølling-Allerød (B/A) and Pre-Boreal (PB). Gray bands indicate the timing of mwp-1A and mwp-1B) (Lambeck et al., 2014). The pin marks at the bottom represent the age control points of core PS2458-4.

444

446

448

450

452

454

456

5 Discussion

5.1 The HS1 (18.0–14.6 kyr BP), B/A (14.7–12.9 kyr BP) and PB (11.5–9.5 kyr BP)

Our results suggest that the highest MARs of both terrestrial lipid- and lignin-derived materials occurred during the B/A and PB (Fig. 2. b, c, d). High TOC contents were also observed during these periods (Fig. S1b). These periods coincided with stages of rapid sea-level rise, linked with the mwp-1A and -1B that started around 14.7 and 11.5 kyrs BP, respectively, leading to an increase in sea-level of approximately 80 m (Fig. 2l) (Lambeck et al., 2014). The synchronicity of these events suggests that flooding and erosion of the coastal areas played a primary role in remobilizing terrigenous OC from the previously frozen permafrost. The sudden rise in terrigenous biomarker MARs during these periods suggests that the erosion of coastal permafrost occurred relatively fast. For instance, our data indicate that the transition from the HS1 to the warm B/A period was characterized by a nearly threefold increase in the MAR of brGDGTs over a relatively brief period of 1.3 kyr. Subsequently, the shift from the YD to the PB period exhibited an even more pronounced change, with a sevenfold increase in the MAR of brGDGTs occurring within a comparably short timeframe of 1.4 kyr. Similarly to the present-day warming, erosion of permafrost along coastlines happens at exceptionally rapid rates, leading to the collapse of coastal bluffs and the subsequent release of substantial amounts of particulate OM directly into the ocean (Bruhn et al., 2021; Couture et al., 2018; Irrgang et al., 2022). Subsequently, the eroded OM is dispersed, undergoes partial degradation, and is partly redeposited in oceanic sediments (Bröder et al., 2016; Vonk et al., 2014).

Our high MAR results during the PB align well with the data from Tesi et al. (2016), showing high lignin flux during the YD-PB warming period reconstructed from core PC23 from the Laptev Sea (Fig. 2j). This core was retrieved from a water depth of 56 m located about 245 km to the south-west of our core location. High terrigenous OC flux was found by Martens et al. (2020) during the PB-Early Holocene (EH) period from core 31-PC which was recovered at a water depth of 1120 m, about 280 km to the north-east of core PS2458-4, and features overall considerably lower sedimentation rates (Fig 2i). Yet, va ery low OC flux was observed during the B/A period from core 31-PC. The differences in the timings of MARs from nearby cores PC23 and 31-PC might be due to variations in the local sedimentation rates or due to the dating uncertainties. Studies of sediments from the Bering Sea (Meyer et al., 2019), the Sea of Okhotsk (Winterfeld et al., 2018), and the western Laptev Sea (Lin et al., 2024) have also described high accumulation rates of terrigenous materials during the B/A and PB warm periods.

Furthermore, during the B/A and PB, the degradation and erosion of permafrost caused massive amounts of terrestrial organic materials to be remobilized and partially be re-buried in marine sediments in the Laptev Sea. This terrigenous OC has a pre-depositional age of up to 21.5 ^{14}C kyr during the PB (Fig. 2f). The compound-specific radiocarbon results indicate that the terrestrial biomarkers are several thousands of years old and pre-aged. This suggests that the terrestrial OM was remobilized from an old carbon pool compatible with degrading coastal permafrost of Pleistocene origin that was subsequently redeposited at our core site. During the last deglaciation, high pre-depositional ages of ~20 ^{14}C kyr have also been reported from terrestrial OM in the Bering Sea (Meyer et al., 2019) and near Svalbard (Nogarotto et al., 2023). The consistent radiocarbon ages from core HH1109-GC further support the hypothesis put forward by Nogarotto et al. (2023) to justify the deposition of aged, terrigenous-rich OC in the Northern Svalbard region during the onset of the B/A (Fig. 2k). According to Nogarotto et al. (2023), erosion during rapid sea level rise might have remobilized coastal permafrost which was

15

then transported through the Transpolar Drift via sea ice and redeposited in northern Svalbard. This further
498   highlights the significant erosion rates documented in the study region.

500   In contrast, relatively lower MARs of terrigenous biomarkers are recorded during the HS1 compared to the warmer
B/A and PB periods (Fig. 2b, c, d). Although the global sea-level rose by ~ 35 m during HS1, the lower MAR of
502   terrigenous materials might be explained by the colder temperatures prevailing in the Arctic (Shakun et al., 2012),
which prevented massive permafrost thaw during this period. Our reconstructed SST shows an average value of
504   ~ 0.7 °C during the B/A-HS1 period, which is lower compared to the SST reported from core ARA04C/37 from
the Beaufort Sea (Wu et al., 2020). Open water conditions with little sea-ice might explain the higher SST in the
506   Beaufort Sea (Wu et al., 2020). Furthermore, enhanced sea-ice cover in the Laptev Sea as represented by the PIP_{25}
index might explain the low terrigenous accumulations during the HS1 (Fahl and Stein, 2012)(Fig. S1c). Similar
508   findings were also reported for nearby core 31-PC from the continental margin of the Eastern Laptev Sea (Martens
et al., 2020) and from the Bering Sea (Meyer et al., 2019), the western Laptev Sea (Lin et al., 2024) and the Sea
510   of Okhotsk (Winterfeld et al., 2018).

512   The bulk OC pre-depositional ages, representing both terrestrial and marine OM, display the same range of values
as the pre-depositional age of terrigenous materials during the HS1-B/A period (Fig. 2e, f). This implies that bulk
514   OC consists mainly of terrestrial OC during early deglaciation, as also corroborated by more depleted $\delta^{13}C$ values
(Fig. 2g), as well as from other terrestrial biomarker records previously reported from this core (Fahl and Stein,
516   2012; Hörner et al., 2016). This interpretation is further supported by the fact that the core site was very close to
the paleo-coastline around 14 – 16 kyr BP (Fig. 1) at a time when the rate of sea-level change was relatively high
518   (Fig. 2l). Therefore, terrigenous OC from degrading permafrost was eroded, deposited and underwent preservation
in marine sediments at the core site during early deglaciation.

520

The S/V ratio remained relatively stable during the HS1-B/A interval (Fig. 3d), indicating a continued contribution
522   of angiosperm-derived lignin at the time when the core site was close to the coastline (Fig. 1). The C/V ratio (Fig.
3c, 4) showed a slight drop during the warm B/A and PB periods, indicating more woody contribution during
524   periods of rapid sea-level rise, leading to coastal erosion and remobilizing both lignin phenols and lipids from
erosion of deeper deposits as indicated by high MARs (Fig. 2b, c, d). In general, the transfer of vascular plant-
526   derived lignin from land to marine sediment occurs primarily via surface water flow and is dominantly governed
by riverine discharge (Feng et al., 2013). In contrast, long-chain *n*-alkanoic acids originate from the epicuticular
528   waxes of vascular and aquatic plant tissues (Eglinton & Hamilton, 1967), and their presence in the sedimentary
record may indicate the mobilization of belowground terrestrial OM from thawing permafrost in modern Arctic
530   River systems (Feng et al., 2013, 2015). The transport of these *n*-alkanoic acids to the ocean is likely to occur
primarily through erosive processes during periods of shelf inundation (Vonk et al., 2012; Winterfeld et al., 2018).
532   Our results corroborate those of Cao et al. (2023), where the authors suggested that both types of terrestrial
biomarkers are indeed transported to the ocean by the same transport pathway during periods of rapid sea-level
534   rise and shelf flooding.

536 The relatively lower Ad/Al ratios (Fig. 3f, g) during the B/A and PB, on the other hand, correspond to maxima in the MARs of lipids and lignin-derived terrigenous biomarkers (Fig. 2b, c, d). This may indicate better preservation

538 of terrigenous OM during rapid burial, as a consequence of massive coastal erosion due to rapid sea-level rise. Previous studies have also suggested better preservation of OM during B/A and PB (Anderson et al., 2003; Meyer

540 et al., 2019).

542 **5.2 The YD (12.9–11.5 kyr BP)**

Our results reveal a noticeable drop in the terrigenous biomarker MARs values during the YD, corresponding to

544 a reduction in the rate of sea-level rise (Fig. 2l) (Klemann et al., 2015; Lambeck et al., 2014) and a decrease in temperatures as recorded in the NGRIP $\delta^{18}O$ data (Fig. 2o) (Andersen et al., 2004) and in the reconstructed SST

546 (Fig. 2m), indicating colder conditions in the Northern Hemisphere. The lowest reconstructed SST was observed during the YD. At our core site, the average reconstructed SST was approximately -2 °C, which is actually the

548 freezing point of seawater at a salinity of ~35 ppt. In fact, sea-ice increased at our core site during the YD (Fig. S1c), which supported the lowest estimated SST during this period. Moreover, our reconstructed SST from the

550 Laptev Sea was observed to be lower than the average reconstructed SST values reported for the Beaufort Sea during the same interval (Wu et al., 2020). A drop in the MARs of terrestrial biomarkers was also reported from

552 core PS2458-4 (Fahl and Stein, 2012) and from core PS51/154 from the western Laptev Sea (Hörner et al., 2016; Lin et al., 2024).

554

The YD cooling event is believed to have been triggered by a catastrophic drainage of meltwater from Lake

556 Agassiz, which significantly disrupted the AMOC and led to rapid sea-ice expansion (Lowell et al., 2005; Renssen et al., 2015). However, the exact mechanisms and timing of these events remain subjects of ongoing scientific

558 debate and investigation (Norris et al., 2021, and citations therein). A freshwater outburst event at 13 kyr BP in the Laptev Sea was proposed in Spielhagen et al. (2005), to explain a decrease in the planktic foraminifera stable

560 oxygen isotope ($\delta^{18}O$) record of core PS2458-4 and is believed to have occurred at the onset of the YD (Fig. 2h). The YD cold event has been related large-scale effects, as revealed by isotope-based permafrost climate records

562 in northern Alaska (Meyer et al., 2010). Studies on the reconstruction of sea ice coverage in the eastern Fram Strait, as reported by Müller and Stein (2014), indicate that maximum sea ice conditions occurred in this region

564 during the YD cold period. Additionally, sediment cores from the southern Fram Strait reveal an expansion of sea ice between 12.8 and 11.8 kyr BP (Cabedo-Sanz et al., 2013; Knies, 2005; Müller and Stein, 2014; Ślubowska-

566 Woldengen et al., 2008). These findings align with evidence of a weakened AMOC and highlight the extensive climatic impacts associated with the YD cold event.

568

By applying our age-depth model with ∆R value of 345 ± 60 ^{14}C years on the planktic oxygen isotope record of

570 core PS2458-4, the freshwater excursion is observed to occur ~ 12.0 kyr BP, right in the middle of the YD. Another record (core JPC15) from the Beaufort Sea, from the North American Arctic sector revealed that a drop

572 in the $\delta^{18}O$ values also occurred during the YD starting from 12.9 kyr BP and was related to the floodwater event through the Mackenzie River (Keigwin et al., 2018). The evident peaks in the MARs of terrigenous biomarkers

574 from core JPC15 reflect the YD flood event, when a large quantity of heterogenous sediments was deposited into the Beaufort Sea (Broecker, 2006; Keigwin et al., 2018; Wu et al., 2020, 2022). The decrease in the terrigenous

576   biomarkers MARs during the YD observed in our core from the Laptev Sea, however, suggests that the freshwater outburst might not have originated from the Siberian Arctic sector or the Lena River. If the freshwater outburst

578   had come from the Siberian Arctic, we would have expected a sharp increase in the terrigenous MARs and similar sedimentological features (finely laminated sediments), as described by Keigwin et al. (2018) and Wu et al.

580   (2022). By investigating the hydrogen isotopic composition of palmic acid ($\delta^2 H_{PA}$) as a potential paleohydrographic proxy, Sachs et al. (2018) reported that at the onset of the YD the sea surface salinity values

582   from core PS72/291-2 in the Beaufort Sea dropped from 20 to 16 before increasing to 24 in the early Holocene. This decrease in salinity is suggested to be linked to the Mackenzie River flooding just before the YD event.

584   Similarly, based on $\delta^2 H$ values of dinosterol from core ARA04C/37, Wu et al. (2025) reported a decrease in salinity of approximately 15–24 in the Beaufort Sea during the YD. Salinity reconstructions from core PS2458-

586   4 in the Laptev Sea during YD revealed lower values (18.7–21.8) compared to the modern salinity of ~29, although no systematic changes were observed (Sachs et al., 2018). Moreover, based on sea ice and open-water

588   phytoplankton biomarkers determined in core PS2458-4, enhanced freshwater flux related to the Mackenzie YD flood event might have triggered enhanced sea-ice formation at the Laptev Sea continental margin (Fahl and Stein,

590   2012; Stein et al., 2012), rather than the local freshwater outburst from Siberia proposed by Spielhagen et al. (2005). The final proof about the origin of the freshwater event recorded in the $\delta^{18}O$ of planktic foraminifera in

592   the Laptev Sea core PS2458-4, that is, whether it came from the North American Arctic region or the Siberian Arctic, however, still remains to be resolved.

594

       The low terrigenous MARs have implications for coastal input as well. Specially, during the YD, both the pre-

596   depositional ages of the *n*-alkanoic acids and bulk OC become younger and have broadly similar values (Fig. 2e, f), potentially indicating that bulk OC contains predominantly terrestrial OC. The relatively younger pre-

598   depositional ages of *n*-alkanoic acids (~8.8 to 10.5 ^{14}C kyr) and bulk OC observed during the YD could be explained by a weakening in permafrost degradation in the Siberian hinterland and along the coast due to

600   generalized cooling (Fig. 2o), reduction in the rate of sea-level change (Fig. 2l) and an increase in sea-ice cover at the core site (Fig. S1c). The presence of sea ice can preserve the coast from massive erosion, with a stabilizing

602   effect by creating a protective barrier that restricts wind and wave action along coastlines, thus minimizing coastal erosion. Furthermore, due to the colder climates, the riverbank erosion might have reduced due to the stabilization

604   of the riverbanks, and therefore preferentially transporting younger terrestrial materials derived from shallower or near-surface deposits. Based on analyses from low density fractions of OC, composed of large plat fragments,

606   from core PC23, Sabino et al. (2024) reported much lower pre-depositional ages of ~ 2.6 ^{14}C kyr during the YD, which could be attributed to the fact that core PC23 was affected mainly by riverine input due to its closer

608   proximity to the coast.

610   Even though there was a prominent drop in the lignin concentration during the YD (Fig. 3b), the relatively high S/V ratio can possibly suggest a different source of enhanced angiosperm input from the southern part of the

612   Siberian hinterland. On the contrary, the lipid terrestrial biomarkers indicate lower MARs during the cold YD. The refreezing of soil during the YD likely inhibited erosion, therefore limiting the subsequent export of lipid

614   terrestrial biomarkers from deeper soil horizons.

616 Tesi et al. (2016) reported that the increased input of OC materials at their core site in the Laptev Sea during the
YD-EH period was transported by the Lena River from the inland catchment area. This corroborates our results

618 about the fact that during the YD terrigenous OC was mainly fluvially transported to the Laptev Sea. The
cutin/lignin ratio (Fig. 3g) shows a sharp increase during the YD, indicating a higher contribution from leaf and

620 needle tissues, which were largely delivered to the ocean via surface runoff.

622 The Ad/Al ratios did not show a sharp increase during the YD, implying that relatively less degradation occurred
during this period of freshwater flooding in the Laptev Sea (Fig. 3e, f). Samples of surface water total suspended

624 matter collected in summer 2009 and 2010 in the Lena River channels, potentially resembling material transported
by a putative YD freshwater outburst, were more degraded (higher Ad/Al ratios ranging from 0.81 to 1.71) in

626 comparison with Pleistocene ice complex samples (lower Ad/Al ratios varying from 0.31 to 0.49) (Winterfeld et
al., 2015). Given that our Ad/Al results exhibit lower values compared to those of the modern Lena River, we

628 propose that the freshwater flooding in the Laptev Sea during the Younger Dryas may have originated from a
source other than the Siberian hinterland. The p-Cd/Fd ratio (Fig. 3h) exhibited a decline during the mid-YD

630 period, indicating a reduction in the degradation of lignin-derived material and suggesting an increased
decomposition of cutin-derived tissues throughout this interval. In addition, a maximum in the 3,5Bd/V ratio

632 occurs during the YD, corresponding to a peak in the Ad/Al ratios. We attribute this occurrence during the cold
YD to variations in the extent of OM decomposition. Taken together, the anomalies documented in several CuO-

634 based proxies might indicate that the contribution from surface runoff was confined to the upper permafrost layer
in response to continental cooling and shallowing of the watertable. Previous studies have indicated that sparse

636 vegetation conditions prevail during the YD cold and dry period (Biskaborn et al., 2012), supporting the idea of a
lower watertable and reduced river flow in northern Siberia during this period.

638

5.3 The Holocene (9.5 – 0 kyr BP)
640 The Holocene is characterized by an evident decrease in the MARs of terrigenous materials, and the values
subsequently remained low throughout the period (Fig. 2b, c, d). These low MARs values suggest that the transfer

642 of terrigenous materials from land to our core site in the Laptev Sea diminished and became stable throughout the
Holocene, aligning with the very low BIT index values (Fig. 2a) and the progressive decrease and constant rate

644 of sea-level rise (Fig. 2l) (Klemann et al., 2015; Lambeck et al., 2014). As sea levels rose from the early
deglaciation into the Holocene, the coastline progressively retreated southward, increasing the distance between

646 the sediment source and the core location (Fig. 1). As a consequence, less terrigenous OM was deposited at the
core site with the increasing distance from the coast, as was also recorded in several other OC and biomarker

648 records (Fahl and Stein, 2012; Hörner et al., 2016; Stein et al., 2001; Stein and Fahl, 2000, 2004). The sea-level
highstand of the Holocene was reached around 5 kyr BP, when the Laptev Sea Shelf was fully inundated, shaping

650 the coastline to the present-day position (Bauch et al., 2001). Moreover, the enhanced sea-ice expansion in the
Laptev Sea during the Holocene (Fig. S1c), supported by low SST (Fig. 2m), might have also prevented further

652 erosion along the coastline and led to a reduction in the export of terrigenous OM to the core site, which was
additionally complicated by the long distance from the coast to the core site.

654

During the Holocene, the pre-depositional ages of the HMW *n*-alkanoic acids ($C_{26:0}$ and $C_{28:0}$) are relatively

656 younger (~ 12.4 to 18.4 ^{14}C kyr) compared to the PB and B/A values (> 17 ^{14}C kyr). The decrease in age is probably due to the reduction in sea-level rise during the Holocene period, which led to a decrease in massive

658 erosion and remobilization of older terrigenous carbon from deeper grounds to marine sediments. Moreover, the core PS2458-4 is located on the Laptev Sea shelf edge, and during the Holocene, the core site was situated about

660 500 km from the Lena delta at an approximate depth of 900 m. If the age at deposition was primarily controlled by lateral transport time across the shelf, we would expect more time for the terrestrial OM to be transported

662 across the shelf with an increase in the age of the terrigenous material. However, our relatively lower pre-depositional ages during the Holocene are in contradiction with the expected increase in age with the cross-shelf

664 transport time as reported by Bröder et al. (2018).

666 The younger terrestrial OM supply during the Holocene is supported by younger pre-depositional ages of HMW *n*-alkanoic acids ($C_{26:0}$ and $C_{28:0}$) (Fig. 2f). However, the increase in the Ad/Al ratios during the Holocene (Fig 3.

668 e, f) does not suggest better preservation of lignin, but it supports the idea of more degraded terrigenous OM arriving at the core site with increasing cross-shelf transport (Bröder et al., 2018). The high values of the 3,5Bd/V

670 and *p*-Cd/Fd ratios observed during the Holocene further corroborate the increase in the degradation of lignin phenols, suggesting progressive degradation of terrigenous OM during cross-shelf transport. From the late YD

672 towards the Holocene, the sea level rose by ~57 m and the rate of sea-level change is then weakened during the Holocene (Klemann et al., 2015; Lambeck et al., 2014). Both the pre-depositional ages of *n*-alkanoic acids and

674 bulk OC were observed to be relatively younger, but the differences in the ages between both records increased. This could be attributed to an increase in the marine contribution introducing younger marine OC, thus making

676 the bulk OC age much younger during the Holocene.

678 Throughout the Holocene, both S/V and C/V ratios exhibited an overall increasing trend, consistent with stable, warm, and wet conditions that favored angiosperm proliferation and increased contributions from non-woody

680 sources in the Lena catchment area. While previous pollen assemblage studies have indicated the appearance of trees and shrubs in the Lena delta region after the Holocene onset (Binney et al., 2009; Schirrmeister et al., 2002),

682 our data do not capture the enhanced contribution from woody angiosperms, which should have been supported by lower C/V ratios. This contrasts with lignin data from core PC23 (Tesi et al., 2016), which showed low C/V

684 ratios implying enhanced contributions of angiosperm and gymnosperm woody material (Fig. 4). Alternatively, if lignin degradation occurs mostly on land, the increase in S/V and C/V ratios might suggest a reduction in the

686 supply of degraded terrigenous OM from land. Our results differ from the lower S/V and C/V ratios observed in cores PC23 and 31-PC during the Holocene (Fig. 4), which have been attributed to riverine transport of terrestrial

688 materials originating from the southern Lena catchment area where gymnosperm trees are more abundant in the boreal forest (Tesi et al., 2016; Winterfeld et al., 2015). Likewise to the results from core PC23, the S/V and C/V

690 ratios from core 31-PC (Fig. 4) also exhibited lower values, suggesting that the terrigenous OM remobilized to this core site during the early Holocene contained mostly angiosperm materials originating from a tundra-like

692 environment and having similar imprints as OM stored in ICD (Martens et al., 2020; Tesi et al., 2014)
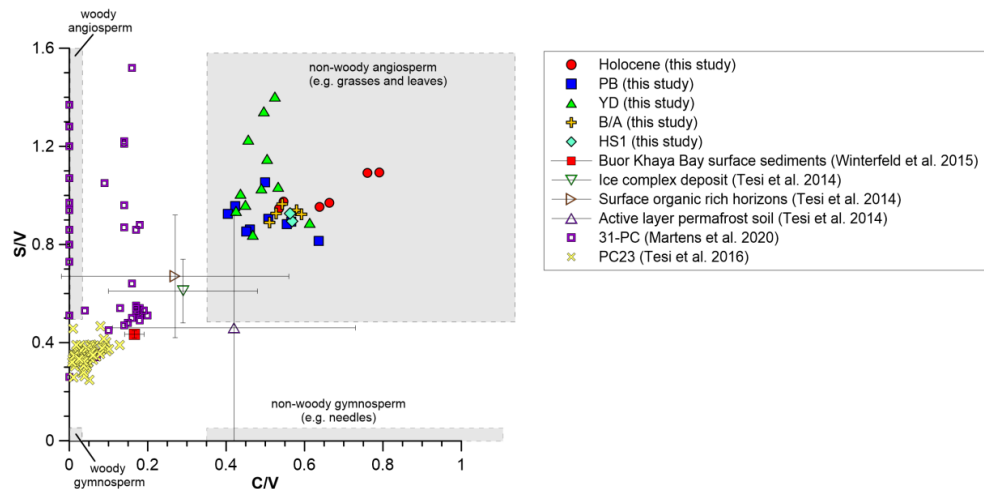
Figure 4. Plot of C/V vs. S/V ratios compared with published data (Martens et al., 2020; Tesi et al., 2014, 2016; Winterfeld et al., 2015)

694

6 Conclusions

696   Our multi-proxy study of core PS2458-4 from the Laptev Sea continental slope provides strong evidence of the dynamic supply of aged terrestrial OM to the ocean during the last deglaciation. The analysis of biomarker MARs,

698   bulk and compound-specific radiocarbon ages, and lignin phenol compositions revealed distinct patterns of terrestrial input across different climatic periods. The highest MARs of terrigenous materials occurred during the

700   warm B/A and PB periods, coinciding with rapid sea-level rise events. This synchronicity strongly suggests that coastal erosion of permafrost played a crucial role in remobilizing aged terrestrial OC. The pre-depositional ages

702   (up to 21.5 ^{14}C kyr) during these periods indicate the release of ancient carbon from degrading permafrost, supporting the growing number of deglacial pre-depositional age records from the Arctic, sub-Arctic and Northern

704   Europe. Both lignin phenols from surface runoff and lipids from erosion of deeper deposits were remobilized during the B/A and PB periods. The terrigenous OM was better preserved during rapid burial as a consequence of

706   massive coastal erosion due to rapid sea-level rise, which has implications for the potential impact of permafrost carbon mobilization on atmospheric greenhouse gas levels.

708

        In contrast, during the cold YD period and concurrently with the previously reported surface water freshening, we

710   observed a significant decrease in terrigenous biomarker MARs, with younger pre-depositional ages. Our results also suggest an enhanced export of grasses and leaves to the ocean likely via surface runoff and rivers. This

712   phenomenon may be attributed to reduced erosion along the riverbanks, potentially resulting from lower ground temperatures that enhanced permafrost stability. The lack of flood layers in our core argues against a flood event

714   from the Lena River as primary cause for the freshwater event. However, this study has not provided any convincing evidence about the origin of the freshwater outburst that occurred during the YD and was recorded in

716   the Laptev Sea. Additional sediment cores from the Siberian Arctic covering the YD period need to be investigated using different geochemical tracers such as authigenic [206]Pb/[204]Pb (Gutjahr et al., 2007), to determine whether this

718 freshwater event was a local occurrence or came from the North American sector of the Arctic. The Holocene is characterized by consistently low MARs of terrigenous materials, reflecting the stabilization of temperature, sea
720 level, and the southward retreat of the coastline.

722 Our results underline the complex interplay between climate change, sea-level fluctuations, and permafrost dynamics in the Arctic. The significant variations in terrigenous export to the ocean observed across different
724 climatic periods demonstrate the sensitivity of Arctic coastal systems to different climate changes. The findings from our study clearly demonstrate that ancient terrestrial OC from permafrost was remobilized during past warm
726 periods, coinciding with rapid sea level rise that caused massive erosion of the Arctic coastline. This unfortunate scenario will likely re-occur over this century due to the predicted warming and sea level rise. Permafrost carbon
728 mobilization has the potential to increase greenhouse gas concentrations in the atmosphere and act as positive climate feedback that might further intensify global warming. Our findings will help refine the understanding of
730 ancient C release and the permafrost carbon feedback in future climate modeling endeavors.

732

734

736

738

740

742

744

746

748

750

752

754

756

Data availability

758

The compound-specific radiocarbon and the bulk OC datasets are available in the supplementary materials. The
760 biomarker and bulk datasets generated and analyzed during the current study will be available in PANGAEA
repository. Additional information related to this study may be requested from the authors.

762

Author contributions

764 G.M designed the study. A.Ni and J.H carried out biomarker analyses, purification of long-chain *n*-alkanoic acids
and the preparation for compound-specific radiocarbon analyses. H.G performed AMS ^{14}C analysis on the
766 MICADAS system and carried out ^{14}C blank correction. T.T and A.No measured δ^{13}C, TOC, lignin and cutin
data. R.S provided the samples for this study. E.Q.A contributed to set-up of the age model. A.Ni drafted the
768 figures and wrote the manuscript draft with the support of G.M. All co-authors provided feedback on the
manuscript at different stages and contributed to the final version of the paper.

770

Competing interests

772 One of the co-authors is currently working as an editorial manager for EGU.

774 **Acknowledgements**

780

782

784

786

788

790

792

794

796

798   **References**

Alves, E. Q., Wong, W., Hefter, J., Grotheer, H., Tesi, T., Gentz, T., Zonneveld, K., and Mollenhauer, G.:
800   Deglacial export of pre-aged terrigenous carbon to the Bay of Biscay, Climate of the Past, 20, 121–136,
       https://doi.org/10.5194/cp-20-121-2024, 2024.
802 Amon, R. M. W., Rinehart, A. J., Duan, S., Louchouarn, P., Prokushkin, A., Guggenberger, G., Bauch, D.,
       Stedmon, C., Raymond, P. A., Holmes, R. M., McClelland, J. W., Peterson, B. J., Walker, S. A., and Zhulidov,
804   A. V.: Dissolved organic matter sources in large Arctic rivers, Geochim Cosmochim Acta, 94, 217–237,
       https://doi.org/10.1016/j.gca.2012.07.015, 2012.
806 Andersen, K. K., Azuma, N., Barnola, J. M., Bigler, M., Biscaye, P., Caillon, N., Chappellaz, J., Clausen, H. B.,
       Dahl-Jensen, D., Fischer, H., Flückiger, J., Fritzsche, D., Fujii, Y., Goto-Azuma, K., Grønvold, K., Gundestrup,
808   N. S., Hansson, M., Huber, C., Hvidberg, C. S., Johnsen, S. J., Jonsell, U., Jouzel, J., Kipfstuhl, S., Landais, A.,
       Leuenberger, M., Lorrain, R., Masson-Delmotte, V., Miller, H., Motoyama, H., Narita, H., Popp, T.,
810   Rasmussen, S. O., Raynaud, D., Rothlisberger, R., Ruth, U., Samyn, D., Schwander, J., Shoji, H., Siggard-
       Andersen, M. L., Steffensen, J. P., Stocker, T., Sveinbjörnsdóttir, A. E., Svensson, A., Takata, M., Tison, J. L.,
812   Thorsteinsson, T., Watanabe, O., Wilhelms, F., and White, J. W. C.: High-resolution record of Northern
       Hemisphere climate extending into the last interglacial period, Nature, 431, 147–151,
814   https://doi.org/10.1038/nature02805, 2004.
     Anderson, P. M., Edwards, M. E., and Brubaker, L. B.: Results and paleoclimate implications of 35 years of
816   paleoecological research in Alaska, Developments in Quaternary Science, 1, 427–440,
       https://doi.org/10.1016/S1571-0866(03)01019-4, 2003.
818 Bauch, H. A., Kassens, H., Erlenkeuser, H., Grootes, P. M., and Thiede, J.: Depositional environment of the
       Laptev Sea (Arctic Siberia) during the Holocene, Boreas, 28, 194–204, https://doi.org/10.1111/j.1502-
820   3885.1999.tb00214.x, 1999.
     Bauch, H. A., Mueller-Lupp, T., Taldenkova, E., Spielhagen, R. F., Kassens, H., Grootes, P. M., Thiede, J.,
822   Heinemeier, J., and Petryashov, V. V.: Chronology of the holocene transgression at the north siberian margin,
       Glob Planet Change, 31, 125–139, https://doi.org/10.1016/S0921-8181(01)00116-3, 2001.
824 Bianchi, T. S. and Canuel, E. A.: Chemical biomarkers in aquatic ecosystems, Princeton University Press,
       Princeton, https://doi.org/10.2138/am.2012.592, 2011.
826 Binney, H. A., Willis, K. J., Edwards, M. E., Bhagwat, S. A., Anderson, P. M., Andreev, A. A., Blaauw, M.,
       Damblon, F., Haesaerts, P., Kienast, F., Kremenetski, K. V., Krivonogov, S. K., Lozhkin, A. V., MacDonald, G.
828   M., Novenko, E. Y., Oksanen, P., Sapelko, T. V., Väliranta, M., and Vazhenina, L.: The distribution of late-
       Quaternary woody taxa in northern Eurasia: evidence from a new macrofossil database, Quat Sci Rev, 28, 2445–
830   2464, https://doi.org/10.1016/j.quascirev.2009.04.016, 2009.
     Biskaborn, B. K., Herzschuh, U., Bolshiyanov, D., Savelieva, L., and Diekmann, B.: Environmental variability in
832   northeastern Siberia during the last ~13,300yr inferred from lake diatoms and sediment-geochemical
       parameters, Palaeogeogr Palaeoclimatol Palaeoecol, 329–330, 22–36,
834   https://doi.org/10.1016/j.palaeo.2012.02.003, 2012.
     Boucsein, B., Fahl, K., and Stein, R.: Variability of river discharge and Atlantic-water inflow at the Laptev Sea
836   continental margin during the past 15,000 years: Implications from maceral and biomarker products,
       International Journal of Earth Sciences, 89, 578–591, https://doi.org/10.1007/s005310000111, 2000.
838 Boucsein, B., Knies, J., and Stein, R.: Organic matter deposition along the Kara and Laptev Seas continental
       margin (eastern Arctic Ocean) during last deglaciation and Holocene: Evidence from organic-geochemical and
840   petrographical data, Mar Geol, 183, 67–87, https://doi.org/10.1016/S0025-3227(01)00249-3, 2002.
     Bröder, L., Tesi, T., Salvadó, J. A., Semiletov, I. P., Dudarev, O. V., and Gustafsson, O.: Fate of terrigenous
842   organic matter across the Laptev Sea from the mouth of the Lena River to the deep sea of the Arctic interior,
       Biogeosciences, 13, 5003–5019, https://doi.org/10.5194/bg-13-5003-2016, 2016.
844 Bröder, L., Tesi, T., Andersson, A., Semiletov, I., and Gustafsson, Ö.: Bounding cross-shelf transport time and
       degradation in Siberian-Arctic land-ocean carbon transfer, Nat Commun, 9, 806,
846   https://doi.org/10.1038/s41467-018-03192-1, 2018.
     Broecker, W. S.: Was the Younger Dryas triggered by a flood?, https://doi.org/10.1126/science.1123253, 2006.
848 Broecker, W. S., Peteet, D. M., and Rind, D.: Does the ocean-atmosphere system have more than one stable mode
       of operation?, Nature, 315, 21–26, https://doi.org/10.1038/315021a0, 1985.
850 Bruhn, A. D., Stedmon, C. A., Comte, J., Matsuoka, A., Speetjens, N. J., Tanski, G., Vonk, J. E., and Sjöstedt, J.:
       Terrestrial Dissolved Organic Matter Mobilized From Eroding Permafrost Controls Microbial Community
852   Composition and Growth in Arctic Coastal Zones, Front Earth Sci (Lausanne), 9, 1–20,
       https://doi.org/10.3389/feart.2021.640580, 2021.
854 Cabedo-Sanz, P., Belt, S. T., Knies, J., and Husum, K.: Identification of contrasting seasonal sea ice conditions
       during the Younger Dryas, Quat Sci Rev, 79, 74–86, https://doi.org/10.1016/j.quascirev.2012.10.028, 2013.

856 Cao, M., Hefter, J., Tiedemann, R., Lembke-Jene, L., Meyer, V. D., and Mollenhauer, G.: Deglacial records of
     terrigenous organic matter accumulation off the Yukon and Amur rivers based on lignin phenols and long-chain
858 n-alkanes, Climate of the Past, 19, 159–178, https://doi.org/10.5194/cp-19-159-2023, 2023.
     Ciais, P., Tagliabue, A., Cuntz, M., Bopp, L., Scholze, M., Hoffmann, G., Lourantou, A., Harrison, S. P., Prentice,
860 I. C., Kelley, D. I., Koven, C., and Piao, S. L.: Large inert carbon pool in the terrestrial biosphere during the
     Last Glacial Maximum, Nat Geosci, 5, 74–79, https://doi.org/10.1038/ngeo1324, 2012.
862 Couture, N. J., Irrgang, A., Pollard, W., Lantuit, H., and Fritz, M.: Coastal Erosion of Permafrost Soils Along the
     Yukon Coastal Plain and Fluxes of Organic Carbon to the Canadian Beaufort Sea, J Geophys Res Biogeosci,
864 123, 406–422, https://doi.org/10.1002/2017JG004166, 2018.
     Eglinton, G. and Hamilton, R. J.: Leaf epicuticular waxes, Science (1979), 156, 1322–1335,
866 https://doi.org/10.1126/science.156.3780.1322, 1967.
     Eglinton, T. I., Aluwihare, L. I., Bauer, J. E., Druffel, E. R. M., and McNichol, A. P.: Gas chromatographic
868 isolation of individual compounds from complex matrices for radiocarbon dating, Anal Chem, 68, 904–912,
     https://doi.org/10.1021/ac9508513, 1996.
870 Ertel, J. R. and Hedges, J. I.: The lignin component of humic substances: Distribution among soil and sedimentary
     humic, fulvic, and base-insoluble fractions, Geochim Cosmochim Acta, 48, 2065–2074,
872 https://doi.org/10.1016/0016-7037(84)90387-9, 1984.
     Fahl, K. and Stein, R.: Biomarkers as organic-carbon-source and environmental indicators in the late quaternary
874 Arctic Ocean: Problems and perspectives, Mar Chem, 63, 293–309, https://doi.org/10.1016/S0304-
     4203(98)00068-1, 1999.
876 Fahl, K. and Stein, R.: Modern seasonal variability and deglacial/Holocene change of central Arctic Ocean sea-ice
     cover: New insights from biomarker proxy records, Earth Planet Sci Lett, 351–352, 123–133,
878 https://doi.org/10.1016/j.epsl.2012.07.009, 2012.
     Fahl, K., Cremer, H., Erlenkeuser, H., Hanssen, H., Hölemann, J., Kassens, H., Knickmeier, K., Kosobokova, K.,
880 Kunz-Pirrung, M., Lindemann, F., Markhaseva, E., Lischka, S., Petryashov, V., Piepenburg, D., Schmid, M.,
     Spindler, M., Stein, R., and Tuschling, K.: Sources and pathways of organic carbon in the modern Laptev Sea
882 (Arctic Ocean): Implications from biological, geochemical and geological data, Polarforschung, 69, 193–205,
     1999.
884 Feng, X., Vonk, J. E., Van Dongen, B. E., Gustafsson, Ö., Semiletov, I. P., Dudarev, O. V., Wang, Z., Montluçon,
     D. B., Wacker, L., and Eglinton, T. I.: Differential mobilization of terrestrial carbon pools in Eurasian Arctic
886 river basins, Proc Natl Acad Sci U S A, 110, 14168–14173, https://doi.org/10.1073/pnas.1307031110, 2013.
     Feng, X., Gustafsson, Holmes, R. M., Vonk, J. E., Van Dongen, B. E., Semiletov, I. P., Dudarev, O. V., Yunker,
888 M. B., MacDonald, R. W., Montluçon, D. B., and Eglinton, T. I.: Multi-molecular tracers of terrestrial carbon
     transfer across the pan-Arctic: Comparison of hydrolyzable components with plant wax lipids and lignin
890 phenols, Biogeosciences, 12, 4841–4860, https://doi.org/10.5194/bg-12-4841-2015, 2015.
     Fütterer, D. K.: The Expedition ARK-IX/4 of RV "Polarstern" 1993, Berichte zur Polarforschung, 149, 244pp.,
892 1993.
     Goñi, M. A. and Hedges, J. I.: The diagenetic behavior of cutin acids in buried conifer needles and sediments from
894 a coastal marine environment, Geochim Cosmochim Acta, 54, 3083–3093, https://doi.org/10.1016/0016-
     7037(90)90124-4, 1990.
896 Goñi, M. A. and Montgomery, S.: Alkaline CuO oxidation with a microwave digestion system: Lignin analyses of
     geochemical samples, Anal Chem, 72, 3116–3121, https://doi.org/10.1021/ac991316w, 2000.
898 Goñi, M. A., Yunker, M. B., MacDonald, R. W., and Eglinton, T. I.: Distribution and sources of organic
     biomarkers in arctic sediments from the Mackenzie River and Beaufort Shelf, Mar Chem, 71, 23–51,
900 https://doi.org/10.1016/S0304-4203(00)00037-2, 2000.
     Gutjahr, M., Frank, M., Stirling, C. H., Klemm, V., van de Flierdt, T., and Halliday, A. N.: Reliable extraction of a
902 deepwater trace metal isotope signal from Fe-Mn oxyhydroxide coatings of marine sediments, Chem Geol, 242,
     351–370, https://doi.org/10.1016/j.chemgeo.2007.03.021, 2007.
904 Heaton, T. J., Köhler, P., Butzin, M., Bard, E., Reimer, R. W., Austin, W. E. N., Bronk Ramsey, C., Grootes, P.
     M., Hughen, K. A., Kromer, B., Reimer, P. J., Adkins, J., Burke, A., Cook, M. S., Olsen, J., and Skinner, L. C.:
906 Marine20 - The Marine Radiocarbon Age Calibration Curve (0-55,000 cal BP), Radiocarbon, 62, 779–820,
     https://doi.org/10.1017/RDC.2020.68, 2020.
908 Hedges, J. I. and Mann, D. C.: The characterization of plant tissues by their lignin oxidation products, Geochim
     Cosmochim Acta, 43, 1803–1807, https://doi.org/10.1016/0016-7037(79)90028-0, 1979.
910 Hedges, J. I., Blanchette, R. A., Weliky, K., and Devol, A. H.: Effects of fungal degradation on the CuO oxidation
     products of lignin: A controlled laboratory study, Geochim Cosmochim Acta, 52, 2717–2726,
912 https://doi.org/10.1016/0016-7037(88)90040-3, 1988.
     Hiyama, T., Park, H., Kobayashi, K., Lebedeva, L., and Gustafsson, D.: Contribution of summer net precipitation
914 to winter river discharge in permafrost zone of the Lena River basin, J Hydrol (Amst), 616, 128797,
     https://doi.org/10.1016/j.jhydrol.2022.128797, 2023.

916 Holmes, M. L. and Creager, J. S.: Holocene History of the Laptev Sea Continental Shelf, in: Marine Geology and
Oceanography of the Arctic Seas, 211–229, https://doi.org/10.1007/978-3-642-87411-6_9, 1974.

918 Holmes, R. M., McClelland, J. W., Peterson, B. J., Tank, S. E., Bulygina, E., Eglinton, T. I., Gordeev, V. V.,
Gurtovaya, T. Y., Raymond, P. A., Repeta, D. J., Staples, R., Striegl, R. G., Zhulidov, A. V., and Zimov, S. A.:
920 Seasonal and Annual Fluxes of Nutrients and Organic Matter from Large Rivers to the Arctic Ocean and
Surrounding Seas, Estuaries and Coasts, 35, 369–382, https://doi.org/10.1007/s12237-011-9386-6, 2012.

922 Hopmans, E. C., Weijers, J. W. H., Schefuß, E., Herfort, L., Sinninghe Damsté, J. S., and Schouten, S.: A novel
proxy for terrestrial organic matter in sediments based on branched and isoprenoid tetraether lipids, Earth Planet
924 Sci Lett, 224, 107–116, https://doi.org/10.1016/j.epsl.2004.05.012, 2004.

Hopmans, E. C., Schouten, S., and Sinninghe Damsté, J. S.: The effect of improved chromatography on GDGT-
926 based palaeoproxies, Org Geochem, 93, 1–6, https://doi.org/10.1016/j.orggeochem.2015.12.006, 2016.

Hörner, T., Stein, R., Fahl, K., and Birgel, D.: Post-glacial variability of sea ice cover, river run-off and biological
928 production in the western Laptev Sea (Arctic Ocean) - A high-resolution biomarker study, Quat Sci Rev, 143,
133–149, https://doi.org/10.1016/j.quascirev.2016.04.011, 2016.

930 Houel, S., Louchouarn, P., Lucotte, M., Canuel, R., and Ghaleb, B.: Translocation of soil organic matter following
reservoir impoundment in boreal systems: Implications for in situ productivity, Limnol Oceanogr, 51, 1497–
932 1513, https://doi.org/10.4319/lo.2006.51.3.1497, 2006.

Hugelius, G., Strauss, J., Zubrzycki, S., Harden, J. W., Schuur, E. A. G., Ping, C. L., Schirrmeister, L., Grosse, G.,
934 Michaelson, G. J., Koven, C. D., O'Donnell, J. A., Elberling, B., Mishra, U., Camill, P., Yu, Z., Palmtag, J., and
Kuhry, P.: Estimated stocks of circumpolar permafrost carbon with quantified uncertainty ranges and identified
936 data gaps, Biogeosciences, 11, 6573–6593, https://doi.org/10.5194/bg-11-6573-2014, 2014.

Irrgang, A. M., Bendixen, M., Farquharson, L. M., Baranskaya, A. V., Erikson, L. H., Gibbs, A. E., Ogorodov, S.
938 A., Overduin, P. P., Lantuit, H., Grigoriev, M. N., and Jones, B. M.: Drivers, dynamics and impacts of changing
Arctic coasts, https://doi.org/10.1038/s43017-021-00232-1, 2022.

940 De Jonge, C., Stadnitskaia, A., Hopmans, E. C., Cherkashov, G., Fedotov, A., Streletskaya, I. D., Vasiliev, A. A.,
and Sinninghe Damsté, J. S.: Drastic changes in the distribution of branched tetraether lipids in suspended
942 matter and sediments from the Yenisei River and Kara Sea (Siberia): Implications for the use of brGDGT-based
proxies in coastal marine sediments, Geochim Cosmochim Acta, 165, 200–225,
944 https://doi.org/10.1016/j.gca.2015.05.044, 2015.

Jorgenson, M. T. and Grosse, G.: Remote Sensing of Landscape Change in Permafrost Regions, in: Permafrost
946 and Periglacial Processes, 324–338, https://doi.org/10.1002/ppp.1914, 2016.

Keigwin, L. D., Klotsko, S., Zhao, N., Reilly, B., Giosan, L., and Driscoll, N. W.: Deglacial floods in the Beaufort
948 Sea preceded Younger Dryas cooling, Nat Geosci, 11, 599–604, https://doi.org/10.1038/s41561-018-0169-6,
2018.

950 Keskitalo, K., Tesi, T., Bröder, L., Andersson, A., Pearce, C., Sköld, M., Semiletov, I. P., Dudarev, O. V., and
Gustafsson, Ö.: Sources and characteristics of terrestrial carbon in Holocene-scale sediments of the East
952 Siberian Sea, Climate of the Past, 13, 1213–1226, https://doi.org/10.5194/cp-13-1213-2017, 2017.

Kleiber, H. P. and Niessen, F.: Late Pleistocene Paleoriver Channels on the Laptev Sea Shelf - Implications from
954 Sub-Bottom Profiling, in: Land-Ocean Systems in the Siberian Arctic, 657–665, https://doi.org/10.1007/978-3-
642-60134-7_49, 1999.

956 Klemann, V., Heim, B., Bauch, H. A., Wetterich, S., and Opel, T.: Sea-level evolution of the Laptev Sea and the
East Siberian Sea since the last glacial maximum, Arktos, 1, 1–8, https://doi.org/10.1007/s41063-015-0004-x,
958 2015.

Knies, J.: Climate-induced changes in sedimentary regimes for organic matter supply on the continental shelf off
960 northern Norway, Geochim Cosmochim Acta, 69, 4631–4647, https://doi.org/10.1016/j.gca.2005.05.014, 2005.

Köhler, P., Knorr, G., and Bard, E.: Permafrost thawing as a possible source of abrupt carbon release at the onset
962 of the Bølling/Allerød, Nat Commun, 5, 5520, https://doi.org/10.1038/ncomms6520, 2014.

Köhler, P., Nehrbass-Ahles, C., Schmitt, J., Stocker, T. F., and Fischer, H.: A 156 kyr smoothed history of the
964 atmospheric greenhouse gases CO2, CH4, and N2O and their radiative forcing, Earth Syst Sci Data, 9, 363–387,
https://doi.org/10.5194/essd-9-363-2017, 2017.

966 Kusch, S., Rethemeyer, J., Schefuß, E., and Mollenhauer, G.: Controls on the age of vascular plant biomarkers in
Black Sea sediments, Geochim Cosmochim Acta, 74, 7031–7047, https://doi.org/10.1016/j.gca.2010.09.005,
968 2010.

Lambeck, K., Rouby, H., Purcell, A., Sun, Y., and Sambridge, M.: Sea level and global ice volumes from the Last
970 Glacial Maximum to the Holocene, Proc Natl Acad Sci U S A, 111, 15296–15303,
https://doi.org/10.1073/pnas.1411762111, 2014.

972 Lin, T.-W., Tesi, T., Hefter, J., Grotheer, H., Wollenburg, J., Adolphi, F., Bauch, H., Nogarotto, A., Müller, J., and
Mollenhauer, G.: Environmental controls of rapid terrestrial organic matter mobilization to the western Laptev
974 Sea since the last deglaciation, Climate of the Past Discussions, 2024, 1–26, https://doi.org/10.5194/cp-2024-60,
2024.

976   Lindgren, A., Hugelius, G., Kuhry, P., Christensen, T. R., and Vandenberghe, J.: GIS-based Maps and Area
          Estimates of Northern Hemisphere Permafrost Extent during the Last Glacial Maximum, Permafr Periglac
978   Process, 27, 6–16, https://doi.org/10.1002/ppp.1851, 2016.
          Lindgren, A., Hugelius, G., and Kuhry, P.: Extensive loss of past permafrost carbon but a net accumulation into
980   present-day soils, Nature, 560, 219–222, https://doi.org/10.1038/s41586-018-0371-0, 2018.
          Lobbes, J. M., Fitznar, H. P., and Kattner, G.: Biogeochemical characteristics of dissolved and particulate organic
982   matter in Russian rivers entering the Arctic Ocean, Geochim Cosmochim Acta, 64, 2973–2983,
          https://doi.org/10.1016/S0016-7037(00)00409-9, 2000.
984   Lowell, T. V., Fisher, T. G., Comer, G. C., Hajdas, I., Waterson, N., Glover, K., Loope, H. M., Schaefer, J. M.,
          Rinterknecht, V., Broecker, W., Denton, G., and Teller, J. T.: Testing the Lake Agassiz meltwater trigger for the
986   Younger Dryas, https://doi.org/10.1029/2005EO400001, 2005.
          Lü, X., Liu, X. L., Elling, F. J., Yang, H., Xie, S., Song, J., Li, X., Yuan, H., Li, N., and Hinrichs, K. U.:
988   Hydroxylated isoprenoid GDGTs in Chinese coastal seas and their potential as a paleotemperature proxy for
          mid-to-low latitude marginal seas, Org Geochem, 89–90, 31–43,
990   https://doi.org/10.1016/j.orggeochem.2015.10.004, 2015.
          Mann, P. J., Strauss, J., Palmtag, J., Dowdy, K., Ogneva, O., Fuchs, M., Bedington, M., Torres, R., Polimene, L.,
992   Overduin, P., Mollenhauer, G., Grosse, G., Rachold, V., Sobczak, W. V., Spencer, R. G. M., and Juhls, B.:
          Degrading permafrost river catchments and their impact on Arctic Ocean nearshore processes, Ambio, 51, 439–
994   455, https://doi.org/10.1007/s13280-021-01666-z, 2022.
          Marcott, S. A., Bauska, T. K., Buizert, C., Steig, E. J., Rosen, J. L., Cuffey, K. M., Fudge, T. J., Severinghaus, J.
996   P., Ahn, J., Kalk, M. L., McConnell, J. R., Sowers, T., Taylor, K. C., White, J. W. C., and Brook, E. J.:
          Centennial-scale changes in the global carbon cycle during the last deglaciation, Nature, 514, 616–619,
998   https://doi.org/10.1038/nature13799, 2014.
          Martens, J., Wild, B., Pearce, C., Tesi, T., Andersson, A., Bröder, L., O'Regan, M., Jakobsson, M., Sköld, M.,
1000   Gemery, L., Cronin, T. M., Semiletov, I., Dudarev, O. V., and Gustafsson, Ö.: Remobilization of Old
          Permafrost Carbon to Chukchi Sea Sediments During the End of the Last Deglaciation, Global Biogeochem
1002   Cycles, 33, 2–14, https://doi.org/10.1029/2018GB005969, 2019.
          Martens, J., Wild, B., Muschitiello, F., O'Regan, M., Jakobsson, M., Semiletov, I., Dudarev, O. V., and
1004   Gustafsson, Ö.: Remobilization of dormant carbon from Siberian-Arctic permafrost during three past warming
          events, Sci Adv, 6, 6546–6562, https://doi.org/10.1126/sciadv.abb6546, 2020.
1006   Meyer, H., Schirrmeister, L., Yoshikawa, K., Opel, T., Wetterich, S., Hubberten, H. W., and Brown, J.: Permafrost
          evidence for severe winter cooling during the Younger Dryas in northern Alaska, Geophys Res Lett, 37,
1008   L03501, https://doi.org/10.1029/2009GL041013, 2010.
          Meyer, V. D., Hefter, J., Köhler, P., Tiedemann, R., Gersonde, R., Wacker, L., and Mollenhauer, G.: Permafrost-
1010   carbon mobilization in Beringia caused by deglacial meltwater runoff, sea-level rise and warming,
          Environmental Research Letters, 14, 085003, https://doi.org/10.1088/1748-9326/ab2653, 2019.
1012   Mollenhauer, G., Grotheer, H., Gentz, T., Bonk, E., and Hefter, J.: Standard operation procedures and
          performance of the MICADAS radiocarbon laboratory at Alfred Wegener Institute (AWI), Germany, Nucl
1014   Instrum Methods Phys Res B, 496, 45–51, https://doi.org/10.1016/j.nimb.2021.03.016, 2021.
          Müller, J. and Stein, R.: High-resolution record of late glacial and deglacial sea ice changes in Fram Strait
1016   corroborates ice-ocean interactions during abrupt climate shifts, Earth Planet Sci Lett, 403, 446–455,
          https://doi.org/10.1016/j.epsl.2014.07.016, 2014.
1018   Nicolas, A., Mollenhauer, G., Lachner, J., Stübner, K., Malter, M., Wollenburg, Grotheer, and Adolphi, F.: Precise
          dating of deglacial Laptev Sea sediments via 14C and authigenic 10Be/9 Be – assessing local 14C reservoir
1020   ages, Climate of The Past, 20, 2617–2628, https://doi.org/https://cp.copernicus.org/articles/20/2617/2024/cp-20-
          2617-2024.pdf, 2024.
1022   Nogarotto, A., Noormets, R., Chauhan, T., Mollenhauer, G., Hefter, J., Grotheer, H., Belt, S. T., Colleoni, F.,
          Muschitiello, F., Capotondi, L., Pellegrini, C., and Tesi, T.: Coastal permafrost was massively eroded during the
1024   Bølling-Allerød warm period, Commun Earth Environ, 4, 350, https://doi.org/10.1038/s43247-023-01013-y,
          2023.
1026   Norris, S. L., Garcia-Castellanos, D., Jansen, J. D., Carling, P. A., Margold, M., Woywitka, R. J., and Froese, D.
          G.: Catastrophic Drainage From the Northwestern Outlet of Glacial Lake Agassiz During the Younger Dryas,
1028   https://doi.org/10.1029/2021GL093919, 2021.
          Otto, A. and Simpson, M. J.: Evaluation of CuO oxidation parameters for determining the source and stage of
1030   lignin degradation in soil, Biogeochemistry, 80, 121–142, https://doi.org/10.1007/s10533-006-9014-x, 2006.
          Ramsey, C. B.: Bayesian analysis of radiocarbon dates, Radiocarbon, 51, 337–360,
1032   https://doi.org/10.1017/s0033822200033865, 2009.
          Rantanen, M., Karpechko, A. Y., Lipponen, A., Nordling, K., Hyvärinen, O., Ruosteenoja, K., Vihma, T., and
1034   Laaksonen, A.: The Arctic has warmed nearly four times faster than the globe since 1979, Commun Earth
          Environ, 3, 168, https://doi.org/10.1038/s43247-022-00498-3, 2022.

1036 Reimer, P. J., Austin, W. E. N., Bard, E., Bayliss, A., Blackwell, P. G., Bronk Ramsey, C., Butzin, M., Cheng, H.,
        Edwards, R. L., Friedrich, M., Grootes, P. M., Guilderson, T. P., Hajdas, I., Heaton, T. J., Hogg, A. G., Hughen,
1038 K. A., Kromer, B., Manning, S. W., Muscheler, R., Palmer, J. G., Pearson, C., Van Der Plicht, J., Reimer, R.
        W., Richards, D. A., Scott, E. M., Southon, J. R., Turney, C. S. M., Wacker, L., Adolphi, F., Büntgen, U.,
1040 Capano, M., Fahrni, S. M., Fogtmann-Schulz, A., Friedrich, R., Köhler, P., Kudsk, S., Miyake, F., Olsen, J.,
        Reinig, F., Sakamoto, M., Sookdeo, A., and Talamo, S.: The IntCal20 Northern Hemisphere Radiocarbon Age
1042 Calibration Curve (0-55 cal kBP), Radiocarbon, 62, 725–757, https://doi.org/10.1017/RDC.2020.41, 2020.
        Renssen, H., Mairesse, A., Goosse, H., Mathiot, P., Heiri, O., Roche, D. M., Nisancioglu, K. H., and Valdes, P. J.:
1044 Multiple causes of the Younger Dryas cold period, Nat Geosci, 8, 946–949, https://doi.org/10.1038/ngeo2557,
        2015.
1046 Romanovskii, N. N., Hubberten, H. W., Gavrilov, A. V., Tumskoy, V. E., Tipenko, G. S., Grigoriev, M. N., and
        Siegert, C.: Thermokarst and land-ocean interactions, Laptev Sea region, Russia, Permafr Periglac Process, 11,
1048 137–152, https://doi.org/10.1002/1099-1530(200004/06)11:2<137::AID-PPP345>3.0.CO;2-L, 2000.
        Ruben, M., Marchant, H., Wietz, M., Gentz, T., Strauss, J., Koch, B. P., and Mollenhauer, G.: Microbial
1050 Communities Degrade Ancient Permafrost-Derived Organic Matter in Arctic Seawater, J Geophys Res
        Biogeosci, 129, e2023JG007936, https://doi.org/10.1029/2023JG007936, 2024.
1052 Sabino, M., Gustafsson, Wild, B., Semiletov, I. P., Dudarev, O. V., Ingrosso, G., and Tesi, T.: Feedbacks From
        Young Permafrost Carbon Remobilization to the Deglacial Methane Rise, Global Biogeochem Cycles, 38,
1054 e2024GB008164, https://doi.org/10.1029/2024GB008164, 2024.
        Sachs, J. P., Stein, R., Maloney, A. E., Wolhowe, M., Fahl, K., and Nam, S. il: An Arctic Ocean paleosalinity
1056 proxy from δ2H of palmitic acid provides evidence for deglacial Mackenzie River flood events, Quat Sci Rev,
        198, 76–90, https://doi.org/10.1016/j.quascirev.2018.08.025, 2018.
1058 Salvadó, J. A., Tesi, T., Sundbom, M., Karlsson, E., Krusä, M., Semiletov, I. P., Panova, E., and Gustafsson, Ö.:
        Contrasting composition of terrigenous organic matter in the dissolved, particulate and sedimentary organic
1060 carbon pools on the outer East Siberian Arctic Shelf, Biogeosciences, 13, 6121–6138,
        https://doi.org/10.5194/bg-13-6121-2016, 2016.
1062 Schefuß, E., Eglinton, T. I., Spencer-Jones, C. L., Rullkötter, J., De Pol-Holz, R., Talbot, H. M., Grootes, P. M.,
        and Schneider, R. R.: Hydrologic control of carbon cycling and aged carbon discharge in the Congo River basin,
1064 Nat Geosci, 9, 687–690, https://doi.org/10.1038/ngeo2778, 2016.
        Schirrmeister, L., Siegert, C., Kuznetsova, T., Kuzmina, S., Andreev, A., Kienast, F., Meyer, H., and Bobrov, A.:
1066 Paleoenvironmental and paleoclimatic records from permafrost deposits in the Arctic region of Northern
        Siberia, Quaternary International, 89, 97–118, https://doi.org/10.1016/S1040-6182(01)00083-0, 2002.
1068 Schouten, S., Huguet, C., Hopmans, E. C., Kienhuis, M. V. M., and Sinninghe Damsté, J. S.: Analytical
        methodology for TEX86 paleothermometry by high-performance liquid chromatography/atmospheric pressure
1070 chemical ionization-mass spectrometry, Anal Chem, 79, 2940–2944, https://doi.org/10.1021/ac062339v, 2007.
        Schuur, E. A. G., Bockheim, J., Canadell, J. G., Euskirchen, E., Field, C. B., Goryachkin, S. V., Hagemann, S.,
1072 Kuhry, P., Lafleur, P. M., Lee, H., Mazhitova, G., Nelson, F. E., Rinke, A., Romanovsky, V. E., Shiklomanov,
        N., Tarnocai, C., Venevsky, S., Vogel, J. G., and Zimov, S. A.: Vulnerability of permafrost carbon to climate
1074 change: Implications for the global carbon cycle, https://doi.org/10.1641/B580807, 2008.
        Schuur, E. A. G., Vogel, J. G., Crummer, K. G., Lee, H., Sickman, J. O., and Osterkamp, T. E.: The effect of
1076 permafrost thaw on old carbon release and net carbon exchange from tundra, Nature, 459, 556–559,
        https://doi.org/10.1038/nature08031, 2009.
1078 Schuur, E. A. G., McGuire, A. D., Schädel, C., Grosse, G., Harden, J. W., Hayes, D. J., Hugelius, G., Koven, C.
        D., Kuhry, P., Lawrence, D. M., Natali, S. M., Olefeldt, D., Romanovsky, V. E., Schaefer, K., Turetsky, M. R.,
1080 Treat, C. C., and Vonk, J. E.: Climate change and the permafrost carbon feedback,
        https://doi.org/10.1038/nature14338, 2015.
1082 Schuur, E. A. G., Abbott, B. W., Commane, R., Ernakovich, J., Euskirchen, E., Hugelius, G., Grosse, G., Jones,
        M., Koven, C., Leshyk, V., Lawrence, D., Loranty, M. M., Mauritz, M., Olefeldt, D., Natali, S., Rodenhizer, H.,
1084 Salmon, V., Schädel, C., Strauss, J., Treat, C., and Turetsky, M.: Permafrost and Climate Change: Carbon Cycle
        Feedbacks From the Warming Arctic, https://doi.org/10.1146/annurev-environ-012220-011847, 2022.
1086 Shakun, J. D., Clark, P. U., He, F., Marcott, S. A., Mix, A. C., Liu, Z., Otto-Bliesner, B., Schmittner, A., and Bard,
        E.: Global warming preceded by increasing carbon dioxide concentrations during the last deglaciation, Nature,
1088 484, 49–54, https://doi.org/10.1038/nature10915, 2012.
        Simmons, C. T., Matthews, H. D., and Mysak, L. A.: Deglacial climate, carbon cycle and ocean chemistry
1090 changes in response to a terrestrial carbon release, Clim Dyn, 46, 1287–1299, https://doi.org/10.1007/s00382-
        015-2646-6, 2016.
1092 Sinninghe Damsté, J. S.: Spatial heterogeneity of sources of branched tetraethers in shelf systems: The
        geochemistry of tetraethers in the Berau River delta (Kalimantan, Indonesia), Geochim Cosmochim Acta, 186,
1094 13–31, https://doi.org/10.1016/j.gca.2016.04.033, 2016.

Ślubowska-Woldengen, M., Koç, N., Rasmussen, T. L., Klitgaard-Kristensen, D., Hald, M., and Jennings, A. E.:
1096   Time-slice reconstructions of ocean circulation changes on the continental shelf in the Nordic and Barents Seas
         during the last 16,000 cal yr B.P., Quat Sci Rev, 27, 1476–1492,
1098   https://doi.org/10.1016/j.quascirev.2008.04.015, 2008.
         Spielhagen, R. F., Erlenkeuser, H., and Siegert, C.: History of freshwater runoff across the Laptev Sea (Arctic)
1100   during the last deglaciation, Glob Planet Change, 48, 187–207, https://doi.org/10.1016/j.gloplacha.2004.12.013,
         2005.
1102   Stein, R. and Fahl, K.: Holocene accumulation of organic carbon at the Laptev Sea continental margin (Arctic
         Ocean): Sources, pathways, and sinks, Geo-Marine Letters, 20, 27–36, https://doi.org/10.1007/s003670000028,
1104   2000.
         Stein, R. and Fahl, K.: The Laptev Sea: Distribution, Sources, Variability and Burial of Organic Carbon, in: The
1106   Organic Carbon Cycle in the Arctic Ocean, edited by: Stein, R. and Macdonals, R. W., 213–236, 2004.
         Stein, R., Boucsein, B., Fahl, K., Garcia de Oteyza, T., Knies, J., and Niessen, F.: Accumulation of particulate
1108   organic carbon at the Eurasian continental margin during late Quaternary times: Controlling mechanisms and
         paleoenvironmental significance, Glob Planet Change, 31, 87–104, https://doi.org/10.1016/S0921-
1110   8181(01)00114-X, 2001.
         Stein, R., Fahl, K., and Müller, J.: Proxy reconstruction of Cenozoic Arctic Ocean sea-ice history - From IRD to
1112   IP25-, Polarforschung, 82, 37–71, 2012.
         Strauss, J., Schirrmeister, L., Grosse, G., Fortier, D., Hugelius, G., Knoblauch, C., Romanovsky, V., Schädel, C.,
1114   Schneider von Deimling, T., Schuur, E. A. G., Shmelev, D., Ulrich, M., and Veremeeva, A.: Deep Yedoma
         permafrost: A synthesis of depositional characteristics and carbon vulnerability,
1116   https://doi.org/10.1016/j.earscirev.2017.07.007, 2017.
         Sun, S., Meyer, V. D., Dolman, A. M., Winterfeld, M., Hefter, J., Dummann, W., McIntyre, C., Montluçon, D. B.,
1118   Haghipour, N., Wacker, L., Gentz, T., Van Der Voort, T. S., Eglinton, T. I., and Mollenhauer, G.: 14C Blank
         Assessment in Small-Scale Compound-Specific Radiocarbon Analysis of Lipid Biomarkers and Lignin Phenols,
1120   Radiocarbon, 62, 207–218, https://doi.org/10.1017/RDC.2019.108, 2020.
         Synal, H. A., Stocker, M., and Suter, M.: MICADAS: A new compact radiocarbon AMS system, Nucl Instrum
1122   Methods Phys Res B, 259, 7–13, https://doi.org/10.1016/j.nimb.2007.01.138, 2007.
         Taldenkova, E., Bauch, H. A., Stepanova, A., Dem'yankov, S., and Ovsepyan, A.: Last postglacial environmental
1124   evolution of the Laptev Sea shelf as reflected in molluscan, ostracodal, and foraminiferal faunas, Glob Planet
         Change, 48, 223–251, https://doi.org/10.1016/j.gloplacha.2004.12.015, 2005.
1126   Tanski, G., Wagner, D., Knoblauch, C., Fritz, M., Sachs, T., and Lantuit, H.: Rapid CO2 Release From Eroding
         Permafrost in Seawater, Geophys Res Lett, 46, 11244–11252, https://doi.org/10.1029/2019GL084303, 2019.
1128   Tesi, T., Semiletov, I., Hugelius, G., Dudarev, O., Kuhry, P., and Gustafsson, Ö.: Composition and fate of
         terrigenous organic matter along the Arctic land-ocean continuum in East Siberia: Insights from biomarkers and
1130   carbon isotopes, Geochim Cosmochim Acta, 133, 235–256, https://doi.org/10.1016/j.gca.2014.02.045, 2014.
         Tesi, T., Muschitiello, F., Smittenberg, R. H., Jakobsson, M., Vonk, J. E., Hill, P., Andersson, A., Kirchner, N.,
1132   Noormets, R., Dudarev, O., Semiletov, I., and Gustafsson: Massive remobilization of permafrost carbon during
         post-glacial warming, Nat Commun, 7, 13653, https://doi.org/10.1038/ncomms13653, 2016.
1134   Tesi, T., Belt, S. T., Gariboldi, K., Muschitiello, F., Smik, L., Finocchiaro, F., Giglio, F., Colizza, E., Gazzurra,
         G., Giordano, P., Morigi, C., Capotondi, L., Nogarotto, A., Köseoğlu, D., Di Roberto, A., Gallerani, A., and
1136   Langone, L.: Resolving sea ice dynamics in the north-western Ross Sea during the last 2.6 ka: From seasonal to
         millennial timescales, Quat Sci Rev, 237, 106299, https://doi.org/10.1016/j.quascirev.2020.106299, 2020.
1138   Vandenberghe, J., French, H. M., Gorbunov, A., Marchenko, S., Velichko, A. A., Jin, H., Cui, Z., Zhang, T., and
         Wan, X.: The Last Permafrost Maximum (LPM) map of the Northern Hemisphere: Permafrost extent and mean
1140   annual air temperatures, 25-17ka BP, Boreas, 43, 652–666, https://doi.org/10.1111/bor.12070, 2014.
         Vonk, J. E. and Gustafsson, Ö.: Permafrost-carbon complexities, https://doi.org/10.1038/ngeo1937, 2013.
1142   Vonk, J. E., Sanchez-Garca, L., Van Dongen, B. E., Alling, V., Kosmach, D., Charkin, A., Semiletov, I. P.,
         Dudarev, O. V., Shakhova, N., Roos, P., Eglinton, T. I., Andersson, A., and Gustafsson, A.: Activation of old
1144   carbon by erosion of coastal and subsea permafrost in Arctic Siberia, Nature, 489, 137–140,
         https://doi.org/10.1038/nature11392, 2012.
1146   Vonk, J. E., Semiletov, I. P., Dudarev, O. V., Eglinton, T. I., Andersson, A., Shakhova, N., Charkin, A., Heim, B.,
         and Gustafsson, Ö.: Preferential burial of permafrost-derived organic carbon in Siberian-Arctic shelf waters, J
1148   Geophys Res Oceans, 119, 8410–8421, https://doi.org/10.1002/2014JC010261, 2014.
         Wacker, L., Němec, M., and Bourquin, J.: A revolutionary graphitisation system: Fully automated, compact and
1150   simple, Nucl Instrum Methods Phys Res B, 268, 931–934, https://doi.org/10.1016/j.nimb.2009.10.067, 2010a.
         Wacker, L., Christl, M., and Synal, H. A.: Bats: A new tool for AMS data reduction, Nucl Instrum Methods Phys
1152   Res B, 268, 976–979, https://doi.org/10.1016/j.nimb.2009.10.078, 2010b.

Wacker, L., Bonani, G., Friedrich, M., Hajdas, I., Kromer, B., Němec, M., Ruff, M., Suter, M., Synal, H. A., and
1154   Vockenhuber, C.: Micadas: Routine and high-precision radiocarbon dating, Radiocarbon, 52, 252–262,
https://doi.org/10.1017/S0033822200045288, 2010c.
1156   Weijers, J. W. H., Schouten, S., Spaargaren, O. C., and Sinninghe Damsté, J. S.: Occurrence and distribution of
tetraether membrane lipids in soils: Implications for the use of the TEX86 proxy and the BIT index, Org
1158   Geochem, 37, 1680–1693, https://doi.org/10.1016/j.orggeochem.2006.07.018, 2006.
Wild, B., Shakhova, N., Dudarev, O., Ruban, A., Kosmach, D., Tumskoy, V., Tesi, T., Grimm, H., Nybom, I.,
1160   Matsubara, F., Alexanderson, H., Jakobsson, M., Mazurov, A., Semiletov, I., and Gustafsson, Ö.: Organic
matter composition and greenhouse gas production of thawing subsea permafrost in the Laptev Sea, Nat
1162   Commun, 13, 5057, https://doi.org/10.1038/s41467-022-32696-0, 2022.
Winterfeld, M., Goñi, M. A., Just, J., Hefter, J., and Mollenhauer, G.: Characterization of particulate organic
1164   matter in the Lena River delta and adjacent nearshore zone, NE Siberia - Part 2: Lignin-derived phenol
compositions, Biogeosciences, 12, 2261–2283, https://doi.org/10.5194/bg-12-2261-2015, 2015.
1166   Winterfeld, M., Mollenhauer, G., Dummann, W., Köhler, P., Lembke-Jene, L., Meyer, V. D., Hefter, J., McIntyre,
C., Wacker, L., Kokfelt, U., and Tiedemann, R.: Deglacial mobilization of pre-aged terrestrial carbon from
1168   degrading permafrost, Nat Commun, 9, 3666, https://doi.org/10.1038/s41467-018-06080-w, 2018.
Wu, J., Stein, R., Fahl, K., Syring, N., Nam, S. Il, Hefter, J., Mollenhauer, G., and Geibert, W.: Deglacial to
1170   Holocene variability in surface water characteristics and major floods in the Beaufort Sea, Commun Earth
Environ, 1, 27, https://doi.org/10.1038/s43247-020-00028-z, 2020.
1172   Wu, J., Mollenhauer, G., Stein, R., Köhler, P., Hefter, J., Fahl, K., Grotheer, H., Wei, B., and Nam, S. Il: Deglacial
release of petrogenic and permafrost carbon from the Canadian Arctic impacting the carbon cycle, Nat
1174   Commun, 13, 7172, https://doi.org/10.1038/s41467-022-34725-4, 2022.
Wu, J., Stein, R., Sachs, J. P., Wolhowe, M., Fahl, K., and You, D.: Quantitative Estimates of Younger Dryas
1176   Freshening From Lipid δ2H Analysis in the Beaufort Sea, Geophys Res Lett, 52, e2024GL112485,
https://doi.org/10.1029/2024GL112485, 2025.
1178   Zimov, N. S., Zimov, S. A., Zimová, A. E., Zimová, G. M., Chuprynin, V. I., and Chapin, F. S.: Carbon storage in
permafrost and soils of the mammoth tundra-steppe biome: Role in the global carbon budget, Geophys Res Lett,
1180   36, L02502, https://doi.org/10.1029/2008GL036332, 2009.

1182